ÇUKUROVA UNIVERSITY
INSTITUTE OF NATURAL AND APPLIED SCIENCES

MSc THESIS

Umut KUMLU

NUMERICAL EXAMINATION OF THE IMPACT CHARACTERISTICS OF VEHICLE SIDE DOOR BEAMS

DEPARTMENT OF AUTOMOTIVE ENGINEERING

ADANA, 2022

ÇUKUROVA UNIVERSITY
INSTITUTE OF NATURAL AND APPLIED SCIENCES

NUMERICAL EXAMINATION OF THE IMPACT CHARACTERISTIC OF VEHICLE SIDE DOOR BEAMS

Umut KUMLU

MSc THESIS

DEPARTMENT OF AUTOMOTIVE ENGINEERING

We certify that the thesis titled above was reviewed and approved for the award of degree of the Master of Science by the board of jury on 29/12/2022

……………………...............	………………………………..	…………………………………
Assoc. Prof. Dr. M. Atakan AKAR	Assoc. Prof. Dr. Hasan SERİN	Assoc. Prof. Dr. İlker SUGÖZÜ
SUPERVISOR	MEMBER	MEMBER

This MSc Thesis is written at the Department of Automotive Engineering of Institute of Natural and Applied Sciences of Çukurova University.
Registration Number:

Prof. Dr. Sadık DİNÇER
Director
Institute of Natural and Applied Sciences

This study supported by Çukurova University Scientific Research Projects Unit.
Project No: FYL-2021-14033

ABSTRACT

MSc THESIS

NUMERICAL EXAMINATION OF THE IMPACT CHARACTERISTIC OF VEHICLE SIDE DOOR BEAMS

Umut KUMLU

ÇUKUROVA UNIVERSITY
INSTITUTE OF NATURAL AND APPLIED SCIENCES
DEPARTMENT OF AUTOMOTIVE ENGINEERING

Supervisor : Assoc. Prof. Dr. M. Atakan AKAR
2nd Supervisor : Assist. Prof. Dr. Şafak YILDIZHAN
Year: 2022, Pages: 67
Jury : Assoc. Prof. Dr. M. Atakan AKAR
: Assoc. Prof. Dr. Hasan SERİN
: Assoc. Prof. Dr. İlker SUGÖZÜ

In side vehicle accidents, there is very small distance between the impactor and the passenger. In such accidents, car manufacturers place impact energy absorber beams inside the door so that the passengers do not suffer from loss of life or major injures. In this study, the crashworthiness performances of impact energy absorber beams were investigated. Comparisons were made by changing the thickness, materials, angles, and cross-sections of the beams. Among the materials used (AL6061-T6 and A36 steel), AL6061-T6 material stood out with its high Specific Energy Absorption (SEA) value, low reaction force, and low permanent deformation performance. The best Velocity Absorption Time (VAT) value was obtained in the combination where the angle between the two beams defined by A36 steel was 25° degrees. It has been stated that the hexagonal cross-section door beam used is superior to the circular beam and is open to improvement.

Key Words: Crashworthiness, Side door beam, Impact energy absorption, Finite element method, SEA, Velocity absorption time

ÖZ

YÜKSEK LİSANS TEZİ

ARAÇ YAN KAPI KİRİŞLERİNİN ÇARPMA ÖZELLİKLERİNİN NUMERİK OLARAK İNCELENMESİ

Umut KUMLU

ÇUKUROVA ÜNİVERSİTESİ
FEN BİLİMLERİ ENSTİTÜSÜ
OTOMOTİV MÜHENDİSLİĞİ ANABİLİM DALI

Danışman : Doç. Dr. M. Atakan AKAR
2. Danışman : Dr. Öğr. Üyesi Şafak YILDIZHAN
Yıl: 2022, Sayfa: 67
Jüri : Doç Dr. M. Atakan AKAR
: Doç. Dr. Hasan SERİN
: Doç. Dr. İlker SUGÖZÜ

Yandan araç kazalarında çarpma tertibatı ile yolcu arasındaki mesafe çok kısadır. Bu tür kazalarda otomobil üreticileri yolcuların can kaybı veya büyük bir zarar görmemesi için kapı içlerine darbe emici kirişler yerleştirmektedir. Bu çalışmada, darbe enerjisi emici kirişlerin çarpmaya dayanıklılık performansları incelenmiştir. Kirişlerin kalınlıkları, malzemeleri, açıları ve kesitleri değiştirilerek karşılaştırmalar yapılmıştır. Kullanılan malzemeler arasında (AL6061-T6 ve A36 çelik), AL6061-T6 malzemesi yüksek Spesifik Enerji Absorbsiyon (SEA) değeri, düşük reaksiyon kuvveti ve düşük kalıcı deformasyon performansı ile öne çıktı. En iyi Hız Soğurma Süresi (VAT) değeri, A36 çeliği ile tanımlanan iki kiriş arasındaki açının 25° derece olduğu kombinasyonda elde edilmiştir. Kullanılan altıgen kesitli kapı kirişinin dairesel kirişe göre daha üstün olduğu ve geliştirilmeye açık olduğu belirtilmiştir.

Anahtar Kelimeler: Çarpmaya karşı dayanıklılık, Yan kapı kirişi, Darbe enerjisi absorbsiyon, Sonlu elemanlar yöntemi, SEA, Hız soğurma süresi

EXTENDED ABSTRACT

The automotive sector is one of the cornerstones of our country and world economy and is growing day by day. Considering the latest developments in automotive production, technological developments have made it possible to produce products with high added value in the automotive sector. With these developments, faster, stronger, more efficient, more comfortable and safer vehicles have started to be produced today. Increasing efficiency in vehicles, reducing fuel consumption, minimizing exhaust emissions and factors that threaten human life are among the topics that the automotive industry and researchers work on intensively.

The increase in the number of vehicles with the increase in population has also led to an increase in accidents. Automotive designers and manufacturers create and integrate safety systems to prevent loss of life. These systems are divided into two classes as active and passive systems. Active safety systems aim to prevent vehicles from crashing. Equipment such as brake and lane tracking systems fall into this group. On the other hand, passive safety systems, are equipment placed in vehicles to ensure the safety of passengers in the moment of accidents, and airbags and door beams are in this class.

Considering the statistics, in vehicle accidents, which are one of the cases with the highest number of fatalities in Turkey and in the world, the most common accident type is frontal collision, while the most common accident type is side collision. The high fatality rate in side collisions is due to the small gap between the impact object and the passenger or driver. There are support beams inside the door to prevent this situation. In-door support beams are passive safety equipment that absorbs the energy of the impacted object in the event of an accident and prevents it from being transferred to the passenger.

With today's technology, vehicles have been made more robust to ensure the safety of passengers. There are organizations such as Euro NCAP established to monitor the safety of vehicles. These organizations conduct real tests and examine how passengers are safe. The cost of performing these tests in the automotive industry is very high. For this reason, vehicle designers examine the strength of vehicle parts or structures with simulation programs using the finite element method.

In this study, a crash simulation was performed based on the research and standards in the literature. The aim of the study is to examine the impact energy absorption performance of new vehicle door beam combinations. In these impact simulations, there are a pole impactor and circular and hexagonal beams. In simulations, using 3 different upper beam angles (10°, 20° and 25°), 2 different beam sections (circular and hexagonal), 2 different beam thicknesses (1.4 and 1.8 mm), and 2 different materials (A36 steel and Aluminum 6061-T6) A total of 15 different impact combinations were investigated. Unlike studies in the literature, the focus is on the deformations and absorbed energies that occur after the impactor hits the beams and rebounds. Differently from most previous studies, the deformation is not constant. Before the impactor rebounds, its velocity drops to zero, which is another unique aspect of the operation. The mass of the impactor was determined as 20 kg based on a study. The impactor is defined as 32 km/h, which is the side impact velocity in Euro NCAP standards. Due to this high velocity, the properties of the materials are defined to the geometries using the Johnson-Cook material model. The simulations were carried out with the ANSYS/Explicit Dynamics program using the finite element method. The average element quality of the mesh structures applied to the models was greater than 0.9. Body sizing and Multizone were used as mesh method for the models. The analysis time was set at 20 ms because the impactor crashes into the beams and bounces back during this time. In the results, the energy absorbed by the beams, SEA, reaction forces, velocity absorption time and deformations were investigated. Among the materials used (Aluminum 6061-T6 and A36 steel), Aluminum 6061T6 material stands out with its high Specific Energy Absorption (SEA) value, low reaction force and low permanent deformation performance. The best Velocity Absorption Time (VAT) value was obtained in combination where the angle between the two beams defined by A36 steel was 25°. It is stated that the hexagonal cross section door beam used is superior to the circular beam and is open to improvement. While the highest energy absorption was obtained from the combination of 25A3614C with 743.8 J value, the lowest absorption value was obtained from the combination of 664.23 J with 10AL18C. In general, steels show higher strength than aluminum alloys. It is an expected result that A36 steel undergoes less deformation and absorbs more energy than AL6061-T6 material. Among the beams, the highest SEA value was observed in the combination of 811.48 J/kg and 25AL14, while the lowest SEA value was obtained in the combination of 233.13 J/kg with 10A3618. Thick beams have lower SEA although they absorb higher energy. Increasing the beam angles also increased SEA as it slightly increased the energy absorbed. The highest peak deformation was observed in the combination 10AL14C with 60.93 mm, and the lowest in the combination 25A3618 with 45.52 mm. The lowest value in plastic deformation was found in 25AL18C with 40.27 mm, while the highest value was found in 10A3614C combination. While the peak deformation of AL6061-T6 material is higher, the plastic deformation of A36 material is higher. This explains why the A36 material absorbs more energy. Among the combinations, the highest reaction force showed 10A3618C with a value of 25.2 kN. The lowest reaction force was seen in 25AL14C with a value of 22.55 kN. The lowest VAT value was observed with 9.62 ms in 25A3618C, while the highest value was found in the combination of 20AL14C with 11.88 ms.

GENİŞLETİLMİŞ ÖZET

Otomotiv sektörü, ülkemiz ve dünya ekonomisinin temel taşlarından biridir ve her geçen gün büyümektedir. Otomotiv üretimindeki son gelişmeler dikkate alındığında, teknolojik gelişmeler otomotiv sektöründe katma değeri yüksek ürünlerin üretilmesini mümkün kılmıştır. Bu gelişmelerle birlikte günümüzde daha hızlı, daha güçlü, daha verimli, daha konforlu ve daha güvenli araçlar üretilmeye başlandı. Araçlarda verimliliğin artırılması, yakıt tüketiminin azaltılması, egzoz emisyonlarının ve insan hayatını tehdit eden faktörlerin en aza indirilmesi otomotiv endüstrisinin ve araştırmacılarının yoğun olarak üzerinde çalıştığı konular arasında yer almaktadır.

Nüfus artışıyla beraber artan araç sayısı, kazaların da artmasına sebep olmuştur. Otomotiv tasarımcıları ve üreticileri can kaybını engellemek aracıyla güvenlik sistemleri oluşturmakta ve araçlara entegre etmektedir. Bu sistemler aktif ve pasif sistemler olarak iki sınıfa ayrılmaktadır. Aktif güvenlik sistemleri araçların kaza yapmasını engelleme amacındadır. Fren ve şerit takip sistemleri gibi donanımlar bu gruba girmektedir. Pasif güvenlik sistemleri ise kazaların gerçekleştiği anda yolcuların güvenliğini sağlamak amacıyla araçlara yerleştirilen donanımlardır ve hava yastıkları ve kapı içi kirişler bu sınıfta bulunmaktadır.

İstatistikler ele alındığında Türkiye'de ve dünyada en çok can kaybı yaşanan vakalardan bir olan araç kazalarında, en sık görülen kaza tipi önden çarpışma olurken, en çok can kaybı yaşanan kaza tipi ise yandan çarpışma olarak göze çarpmıştır. Yandan çarpışmalardaki ölüm oranının yüksek olmasının sebebi, çarpan nesne ile yolcu veya şoför arasındaki boşluğun az olmasıdır. Bu durumu engellemek için kapı içinde destek kirişleri bulunmaktadır. Kapı içi destek kirişler kaza anında çarpan cismin enerjisi emen ve yolcuya aktarılmasını engelleyen bir pasif güvenlik donanımıdır.

Günümüz teknolojisiyle, yolcuların güvenliğini sağlamak için araçlar daha sağlam hale getirilmiştir. Araçların güvenliğini denetlemek için kurulan Euro

NCAP gibi kuruluşlar bulunmaktadır. Bu kuruluşlar gerçek testler gerçekleştirerek yolcuların güvenliğinin nasıl sağlandığını inceler. Otomotiv sektöründe bu testleri gerçekleştirme maliyeti çok yüksektir. Bu nedenle araç tasarımcıları, sonlu elemanlar metodu kullanan simülasyon programlarıyla araç parçalarının veya yapılarının dayanımını incelemektedir.

Bu çalışmada, literatürdeki araştırmalara ve standartlara dayanarak bir çarpışma simülasyonu gerçekleştirilmiştir. Çalışmanın amacı, yeni araç kapı kirişi kombinasyonlarının darbe enerjisi yutma performanslarının incelenmesidir. Bu çarpışma simülasyonlarında, dairesel ve altıgen kesitli kirişlere bir direk çarpma tertibatı çarptı. Simülasyonlarda 3 farklı üst kiriş açısı(10°, 20°ve 25°) , 2 farklı kiriş kesiti(dairesel ve altıgen), 2 farklı kiriş kalınlığı(1,4 ve 1,8 mm) ve 2 farklı malzeme(A36 çeliği ve Alüminyum 6061-T6) kullanılarak toplam 15 farklı darbe kombinasyonu incelenmiştir. Literatürdeki çalışmalardan farklı olarak, çarpma tertibatının kirişlere çarpıp geri sekmesinden sonra oluşan deformasyonlar ve emilen enerjiler üzerinde durulmaktadır. Önceki çalışmaların çoğunun aksine, deformasyon sabit değildir. Çarpma tertibatı geri sekmeden önce hızı sıfıra düşer ve bu, çalışmanın başka bir benzersiz yönüdür. Çarpma tertibatının kütlesi bir çalışmaya dayandırılarak 20 kg olarak belirlenmiştir. Çarpan cisme Euro NCAP standartlarındaki yandan çarpma hızı olan 32 km/h tanımlanmıştır. Bu hızın yüksek olması sebebiyle malzemelerin özellikleri Johnson-Cook malzeme modeli kullanılarak geometrilere tanımlanmıştır. Simülasyonlar, sonlu elemanlar metodu kullanılan ANSYS/Explicit Dynamics programıyla gerçekleştirilmiştir. Modellere uygulanan ağ yapılarının ortalama kalitesi 0.9'dan büyük olmuştur. Modellere mesh metodu olarak body sizing ve Multizone kullanılmıştır. Analiz süresi 20 ms olarak belirlenmiştir çünkü çarpma tertibatı bu süre içinde kirişlere çarpıp geri dönmektedir. Sonuçlarda kirişlerin absorbe ettiği enerji, SEA, reaksiyon kuvvetleri, hız soğurma süresi ve deformasyonlar incelenmiştir. Kullanılan malzemeler arasında (Alüminyum 6061-T6 ve A36 çelik), Alüminyum 6061-T6 malzemesi yüksek Spesifik Enerji Absorbsiyon (SEA) değeri, düşük reaksiyon kuvveti ve düşük kalıcı deformasyon performansı ile ön plana çıkmıştır. En iyi Hız Soğurma Süresi (VAT) değeri, A36 çeliği ile tanımlanan iki kiriş arasındaki açının 25° derece olduğu kombinasyonda elde edilmiştir. Kullanılan altıgen kesitli kapı kirişinin dairesel kirişe göre daha üstün olduğu ve geliştirilmeye açık olduğu belirtilmiştir. En yüksek enerji absorbsiyon 743,8 J değeri ile 25A3614C kombinasyonundan elde edilirken, en düşük absorbe değeri 664,23 J ile 10AL18C kombinasyonu elde edilmiştir. Genel olarak çelikler, alüminyum alaşımlarına göre daha yüksek mukavemet göstermektedir. A36 çeliğinin AL6061-T6 malzemesine göre daha az deformasyona uğraması ve daha fazla enerji emmesi beklenen bir sonuçtur. Kirişler arasında en yüksek SEA değeri 811,48 J/kg ile 25AL14 kombinasyonunda gözlenirken, en düşük SEA değeri 233,13 J/kg ile 10A3618 kombinasyonunda elde edildi. Kalın kirişler daha yüksek enerji emmelerine rağmen daha düşük SEA'ya sahiptir. Kiriş açılarının arttırılması, emilen enerjiyi biraz arttırdığı için SEA'yı da arttırdı. En yüksek tepe deformasyon 60,93 mm ile 10AL14C kombinasyonunda, en düşük ise 45,52 mm ile 25A3618 kombinasyonunda gözlendi. Plastik deformasyonda en düşük değer 40,27 mm ile 25AL18C'de bulunurken, en yüksek değer 10A3614C kombinasyonunda bulundu. AL6061-T6 malzemesinin tepe deformasyonu daha yüksek iken, A36 malzemesinin plastik deformasyonu daha yüksektir. Bu, A36 malzemesinin neden daha fazla enerji emdiğini açıklamaktadır. Kombinasyonlar arasında en yüksek reaksiyon kuvveti 25, 2 kN değeri ile 10A3618C'yi göstermiştir. En düşük reaksiyon kuvveti 22,55 kN değeri ile 25AL14C'de görülmüştür. En düşük VAT değeri 9,62 ms ile 25A3618C'de gözlenirken, en yüksek değer 11,88 ms ile 20AL14C kombinasyonunda bulundu.

ACKNOWLEDGEMENTS

Firstly and foremostly, I would like to express my sincere gratitude to my supervisor Assoc. Prof. Dr. Mustafa Atakan AKAR for his continuous support, patience, motivation, and wisdom. Thanks to his mentoring skills and guidance, I managed to complete the research and writing of this thesis. I am grateful to him not only for being a great supervisor also being a lifetime mentor.

I am thankful to my second advisor Asst. Prof. Dr. Şafak YILDIZHAN for his helps throughout the experiments. His support and advices have considerably contributed to my thesis.

I also thank to other jury members Assoc. Prof. Dr. Hasan SERİN and Assoc. Prof. Dr. İlker SUGÖZÜ for evaluating my thesis.

I specially thank to Prof. Dr. Mustafa ÖZCANLI, Asst. Prof. Dr. Erdi TOSUN, Asst. Prof. Dr. Tayfun ÖZGÜR, Res. Asst. Berkay KARAÇOR and Res. Asst. Ali Cem YAKARYILMAZ for their help and valuable advices throughout my study.

I wish to thank all staff of Automotive Engineering and Head of Automotive Engineering Department, Prof. Dr. Ali KESKİN.

Last but not least, my parents, Necdet KUMLU, Senem KUMLU, and my brother, Uğur KUMLU. I wouldn't have succeeded my thesis without their support and encouragement.

And finally thanks again to my girlfriend who has never stopped supporting me through my life, I would like to express my deepest gratitude to Esra TANLAK

CONTENTS **PAGE**

LIST OF FIGURES **PAGE**

LIST OF TABLES **PAGE**

ABBREVIATIONS

TurkStat	:	Turkish Statistical Institute
ACEA	:	European Automobile Manufacturers' Association
WHO	:	World Health Organization
TGHD	:	Turkish General Directorate of Highways
ABS	:	Anti-Lock Braking System
ESP	:	Electronic Stability Program
EBD	:	Electronic Brake Force Distribution
BIW	:	Body in White
Euro NCAP	:	European New Car Assessment Program
NHTSA	:	National Highway Traffic Safety Administration
IIHS	:	Insurance Institute for Highway Safety
UN-ECE R95	:	United Nations Economic Commission for Europe Regulation 95
FEM	:	Finite Element Method
EA	:	Energy Absorption
SEA	:	Specific Energy Absorption
CFE	:	Crushing Force Efficiency
PCF	:	Peak Crushing Force
MOD	:	Multiobjective Optimization Design
AL-6061-T6	:	Alloy Aluminum 6061-T6

XIX

1. INTRODUCTION

The automotive sector is one of the cornerstones of our country and world economy and is growing day by day. Considering the latest developments in automotive production, technological advances have made it possible to produce products with high added value in the automotive sector. With these advances, vehicles have begun to be produced today that are faster, stronger, more efficient, more comfortable, and safer. Increasing efficiency in vehicles, reducing fuel consumption, minimizing exhaust emissions, and minimizing the factors that threaten human life are among the issues that the automotive industry and researchers work on intensively (Gaylor, 2013).

With the rapid population growth, the number of actively used vehicles in our world and our country is increasing day by day. According to the Turkish Statistical Institute (TurkStat). data shown in Figure 1.1, while the number of vehicles registered for traffic in Turkey in 2002 was 8655170, this number reached 24144857 in 2020. According to these data, the number of vehicles has increased approximately 2.5 times in 18 years (TurkStat, 2020). Besides, according to the report published by The European Automobile Manufacturers' Association (ACEA) in 2021, the number of vehicles in Europe has approached 400 million (ACEA, 2021). While the majority of these vehicles are passenger cars, the increase in the number of minibuses and buses is also striking. This increase in the number of vehicles has made it inevitable to increase the number of accidents.

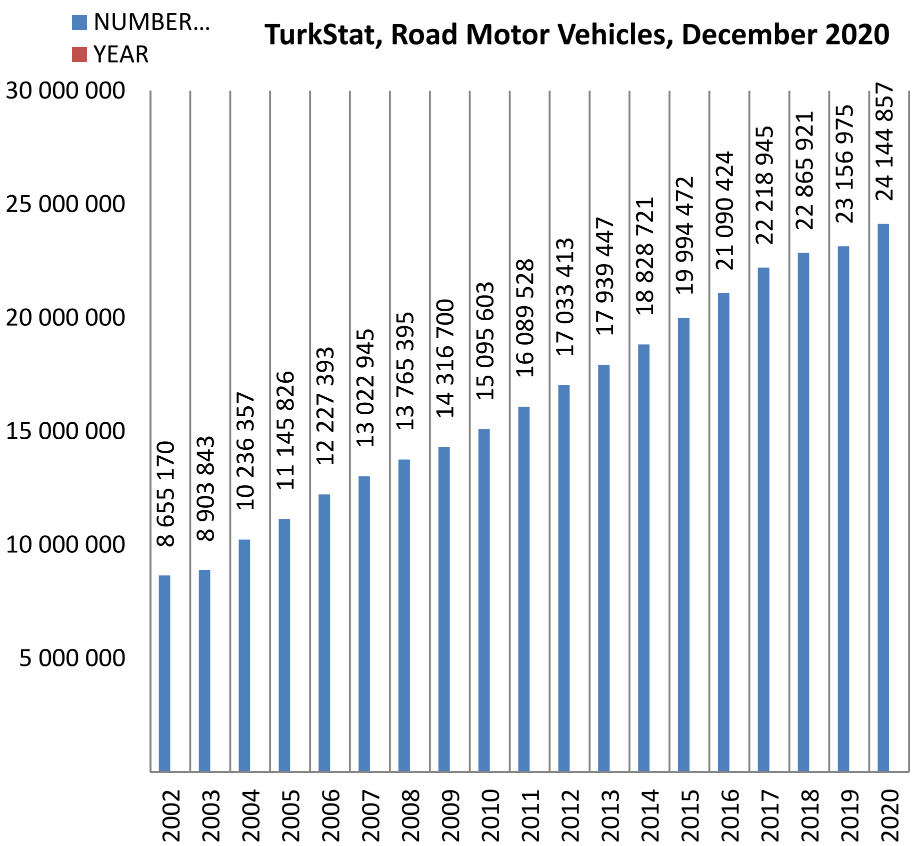

Figure 1.1. TurkStat, Road Motor Vehicles, December 2020 (TurkStat, 2020)

Vehicle accidents, one of the problems brought about by the increase in the number of vehicles, create great problems today. The World Health Organization (WHO) has explained the relationship between the death rate in vehicle accidents, which cause serious loss of life and property, and the increasing number of vehicles between the years 2000-2016, as shown in Figure 1.2. Besides, statistical data showing that road traffic accidents are one of the leading causes of death in the world can be seen in Table 1.1 (WHO, 2018).

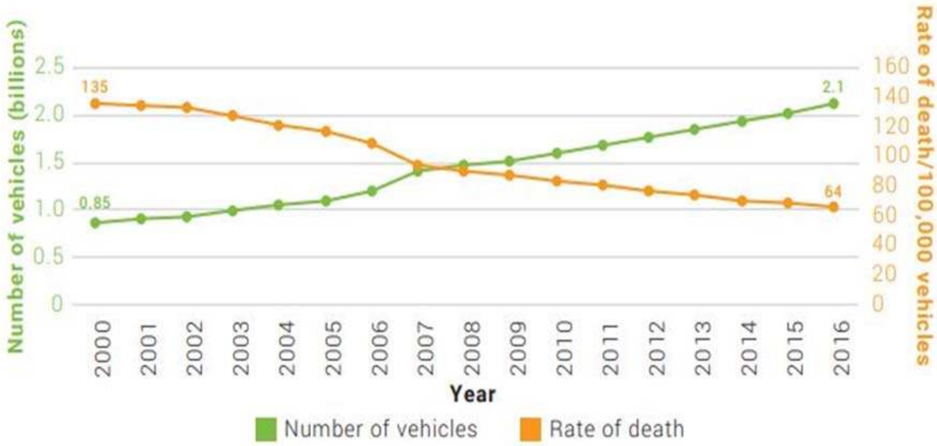

Figure 1.2. Number of motor vehicles and rate of road traffic death per 100,000 vehicles: 2000–2016 (WHO, 2018)

Table 1.1. Leading causes of death, all ages, 2016 (WHO, 2018)

LEADING CAUSES OF DEATH, ALL AGES, 2016		
Rank	**All causes**	**% of total deaths**
1	Ischaemic heart disease	16.6
2	Stroke	10.2
3	Chronic obstructive pulmonary disease	5.4
4	Lower respiratory infections	5.2
5	Alzheimer's disease and other dementias	3.5
6	Trachea, bronchus, lung cancers	3
7	Diabetes mellitus	2.8
8	**Road traffic injuries**	**2.5**
9	Diarrhoeal diseases	2.4
10	Tuberculosis	2.3

Vehicle accident types vary in the direction of impact, the object hit and the movement of the object. Sometimes, while drivers impact with other vehicles from the side with their vehicles, sometimes they may impact oncoming vehicles. In addition to these, it is observed that vehicles can sometimes impact a stationary obstacle and sometimes a moving animal. According to the data published by the Turkish General Directorate of Highways (TGHD) in 2020, the most common type of crash is a side impact. Side collisions are followed by accident types such as getting out of the road, rolling over, and impacting a pedestrian. These statistical data are shown in Table 1.2 (TGHD, 2020).

Table 1.2. Traffic accidents with death and injury by types of occuration in Turkey–2020 (TGHD, 2020)

TRAFFIC ACCIDENTS WITH DEATH AND INJURY BY TYPES OF OCCURATION IN TURKEY - 2020						
ACCIDENTAL TYPE	**RURAL**		**URBAN**		**TOTAL**	
	Number of Accidents	**%**	**Number of Accidents**	**%**	**Number of Accidents**	**%**
Side Impact or Side Collision	41444	36.4	5058	13.89	46502	30.96
Getting Out of the Road	8027	7.05	14134	38.82	22161	14.75
Pedestrian Impact	20913	18.37	908	2.49	21821	14.52
Roll Over and Skid	11944	10.49	5247	14.41	17191	11.44
Rear Impact	11667	10.25	4966	13.64	16633	11.07
Opposing Impact	7233	6.35	2091	5.74	9324	6.2
Impact to Obstacle	6094	5.35	2387	6.56	8481	5.64
Side by Side Impact	1707	1.5	340	0.93	2047	1.36
Impact to Stationary Vehicle	1703	1.5	344	0.94	2047	1.36
Person Falling from Vehicle	1076	0.94	157	0.43	1233	0.82
Impact into Parked Vehicle	1103	0.97	83	0.23	1186	0.79
Multiple-Vehicle Collision	530	0.46	200	0.55	730	0.48
Impact to Animals	381	0.33	473	1.3	854	0.57
Object Falling from Vehicle	41	0.04	24	0.07	65	0.04
TOTAL	**113863**	**100**	**36412**	**100**	**150275**	**100**

As seen in statical data, side-impact crashes account for a major share of all the automotive crashes in Turkey and in the World. As the side of the vehicle has very little room to absorb energy and shield the occupants, there is a need to have a structure that provides a substantial crumple zone. Todays, automakers are providing airbags in addition to strengthening the structure. A many as six airbags are provided to protect the passengers at the time of incidence. The airbags are more of a fail-safe measure, the major concern is the strength of the structure of the vehicle (Sharma, 2018).

The resistance of vehicle to impact indicates the safety of vehicle and is defined by the term crashworthiness. Crashworthiness refers to the ability of vehicle to protect itself during a collision. Vehicle designers and engineers in today's automotive industry attach great importance to the crashworthiness of the vehicle. The safety of the vehicle continues to be improved by the manufacturers due to the large losses as a result of vehicle accidents. The purpose of safety systems, which are divided into two groups as active and passive safety technologies, is to prevent collisions and to reduce the effects of collisions (Gaylor, 2013).

Todays, with the development of technology, modern cars are equipped with much technological equipment designed to prevent accidents from occurring and to keep passengers and pedestrians as safe as possible in the event of an accident. These security systems in vehicles are basically divided into two as active and passive. Active safety systems are the systems and equipment related to the time before the accident that reduces the probability of the accident occurring. As an example of this type of safety equipment; Electronic security systems such as parking sensors, Anti-Lock Braking System (ABS), Electronic Stability Program (ESP), and Electronic Brake Force Distribution (EBD) can be given. More complex and advanced systems, such as radar-guided collision avoidance programs that scan the roads for impending danger, are also beginning to be integrated into more expensive executive and sports vehicles. Passive safety equipments, on the other hand, are a system related to the moment of the accident that reduces the possibility of death and injury for those inside and outside the vehicle at the time of the accident. Examples of such passive safety include good suspension, rigid chassis, good steering and brakes, as well as seat belts and bolsters, airbags, and energy-absorbing or energy-consuming structures in a vehicle chassis or doors. Support beams inside the door or bumper parts at the front of the vehicle can be given as examples of shock-absorbing components made of materials with high energy absorption. The use of materials that provide energy absorption varies depending on where it is needed. In the examples shown in Figure 1.3, the highest strength steel surrounds the passenger compartment, giving occupants the best possible protection against side impacts and rollover collisions, while lower strength steel is placed in areas where crumpling is desired to absorb energy during a collision. Active safety equipment is the first defense against a collision as it is a preventive measure and is of great interest to automobile manufacturers, but passive safety equipment can be said to save lives because it can prevent injury and loss of life in any accident (Long, 2015).

Figure 1.3. Mixed materials BIW (Body in White) for Chevrolet Malibu and Cadillac CT6 (courtesy of General Motors) (Liu et al., 2018)

Shock absorbing beams in the vehicle door, which is one of the passive safety equipment, can protect the driver from injury or loss of life in accidents where vehicles are hit from the side. Increasing the number of vehicle door beams made of steel such as different types of aluminum (AL6061, AL6060 etc.) or A36, changing their positions, or increasing the absorption ability by being produced from different materials can prevent the transfer of energy to the driver in case of side impacts of the vehicles (Ghadianlou and Abdullah, 2013). Examples of different types of vehicle beams are shown in Figure 1.4.

(a) (b)

Figure 1.4. Different types of anti-intrusion apparatus, (a) impact beam (Hyundai Azera, 2015), and (b) corrugated steel (Meritor, 2015)

The increasing number of vehicles with the growth in the automotive industry has created the need to check the safety of the vehicles. Various standards and regulations have been established in order to control the safety of the cars produced. Various institutions and regulatory organizations such as the European New Car Assessment Program (Euro NCAP), the National Highway Traffic Safety Administration (NHTSA), and the Insurance Institute for Highway Safety (IIHS) evaluate the vehicles in terms of safety.

Euro NCAP is a European Union (EU) supported program that evaluates vehicle safety performance in accordance with The United Nations Economic Commission for Europe Regulation 95 (UN-ECE R95) in terms of test features, injury criteria, and crash test. It conducts a variety of tests, including front, side, pole, and pedestrian impact testing, with qualitative results defined through a 5-star rating system shown in Table 1.3.

Table 1.3. Different star systems of the Euro NCAP rating (Euro NCAP, 2021a)

EXPLANATION	**STARS RATE**
Overall excellent performance in crash protection and well equipped with comprehensive and robust crash avoidance technology	5 stars safety
Overall good performance in crash protection and all round; additional crash avoidance technology may be present	4 stars safety
At least average occupant protection but not always equipped with the latest crash avoidance features	3 stars safety
Nominal crash protection but lacking crash avoidance technology	2 stars safety
Marginal crash protection and little in the way of crash avoidance technology	1 star safety
Meeting type-approval standards so can legally be sold but lacking critical modern safety technology	0 star safety

Side-impact tests are of 2 types: the vertical impact of the mobile deformable barrier and the side-sloping impact of the fixed pole. The Figure 1.5. shows the side-impact tests in a simplified form.

The mobile deformable barrier side-impact tests are performed at 60 km/h velocity by placing a 75 kg dummy of the driver and 36 and 23 kg child dummies on the rear seats. Luggage load, on the other hand, can exceed 100 kg with the rear and front axle loads.

A total of 81 data collectors (84 in the dual occupancy test) are placed. (35 channels on regions such as the head, upper neck, shoulder joint, scapula, sternum, abdominal cavity, waist, and pelvis of the dummy of the driver, 30 and 13 channels on the child dummies, 2 channels on the b-column, and battery of the vehicle, and 1 channel on the center of gravity of the barrier carrier). These channels measure acceleration, force, moment, linear, and rotational displacement values from their points of attachment.

The weight of the deformable barrier and its carrier is 1400 kg. The height of the barrier is adjusted so that the intersection edge of the upper and lower deformed blocks is 550 mm from the ground. The wheelbase of the barrier carrier is 3000 mm, and the front and rear track widths are 1500 mm (Euro NCAP, 2020b).

Crash tests with a side slope to the rigid mast are performed at 32 km/h velocity using a 75 kg dummy of driver and luggage weights not exceeding 136 kg. The reference of the vehicle hitting the rigid pole makes an angle of 75° with the vehicle's longitudinal axis, passing both through the center point of the head of the driver. A total of 38 channels (41 in 84 in the dual occupancy test) are placed (35 on the driver's dummy, 2 on the vehicle, and 1 on the carrier). The rigid pole is a vertical structure beginning no more than 102 mm above the lowest point of the tires on the striking side of the test vehicle when the vehicle is loaded and extending at least 100 mm above the highest point of the roof of the test vehicle. The rigid pole has a metal structure with a diameter of 254 mm. The acceleration of the carrier during the test should not exceed 1.5 m/s^2 (Ellway et al., 2013; Euro NCAP, 2020a).

(a)

(b)

Figure 1.5. Euro NCAP side crash tests (a) Mobile deformable barrier side-impact tests (b) Oblique pole side impact testing (Euro NCAP, 2021b)

A full-scale crash test is considered the most reliable source of information regarding the structural integrity and safety of motor vehicles. However, the high cost of such tests and difficulties in collecting data has resulted in an increasing interest in the analytical and computational methods of evaluation. With the advancement in computer simulations, full finite element validated vehicle models are being analyzed for different impact scenarios to predict vehicle behavior and occupant response (Yadav, 2006).

In this study, a crash simulation was performed based on the researches in the literature. The aim of the study is to examine the impact energy absorption performances of the new vehicle door beam combinations. In this crash simulations, a pole impactor was impacted to circular and hexagonal cross-sectional beams. A total of 15 different impact combinations were investigated using 3 different upper beam angles, 2 different beam cross-sections 2 different beam thicknesses, and 2 different materials in the simulations. Unlike studies in the literature, the focus is on the deformations and absorbed energies that occur after the impactor hits the beams and bounces back. Contrary to most previous studies, the deformation is not constant. Before the impactor bounces back, its velocity drops back to zero, and this is another unique aspect of the study.

2. LITERATURE SURVEY

With the developments in the automotive field, automobile designers have enabled cars to reach very high speeds by optimizing the engine efficiency and the aerodynamic structure of the vehicle. While this development provided an advantage in terms of time, it caused the passengers to face greater forces at the time of the accident and to receive damages that would cause loss of life. Therefore, researchers have carried out various studies to protect passengers in the event of a crash. An important part of these researches consists of the activities to reveal the lightest material with the best energy absorption ability. Crash simulations were created by testing different materials for chassis, doors, bumpers, and other vehicle components. The designs of vehicle components were shaped in line with these researches.

While the front bumper and shock absorbing crush boxes will be the first to be damaged and absorb the impact in the frontal impacts of the vehicle; The beams on the doors are one of the components that protect the driver in case of side impacts. Therefore, researchers aimed to develop these components in their simulations and research. Marzbanrad et al., by creating a finite element simulation, investigated the energy absorption values of energy absorbing crush boxes with different geometric dimensions. Using steel and aluminum as materials, the researchers compared the energy absorption capabilities of shock absorbers using square, elliptical and circular pipe sections. According to the results obtained by Marzbanrad et al., who included 2 different section sizes and 2 different thickness scenarios in the simulation; While the highest impact absorption ability was observed in the elliptical section, the researchers stated that the narrow section crush boxes absorb higher energy with an increasing thickness(Marzbanrad et al., 2009).

In another study, Li et al., by using TRIP800, Aluminum 6060, and DP800 materials in bumpers and shock absorbers in automobiles, aimed to increase the energy absorption capacity of the components and reduce the weight of these parts. In the created crush simulation, the researchers carried out an optimization study in terms of lightness and strength by filling the interiors of the components with aluminum foam in order to increase energy absorption. Li et al., who included a new design by combining different materials and comparing multi-material design with single-material design in the research, considered the collision criteria and concluded that the combination of multi-material design and aluminum foam and components significantly increased the energy absorption. In addition, they stated that the multi-material design has great potential for optimizing its lightness and energy-absorbing ability (Li et al., 2017).

While Qi et al., by modeling square tubes in 5 different thin-walled structures as single-cell, multicell, tapered, and conical examined their collision behavior with the finite element method, and by producing these structures, they also performed experimental crushing analysis. In these structures, AL6061 Aluminum alloy has been used as a material because it has the ability to absorb high energy. Qi et al., who proceeded with their studies by establishing Specific Energy Absorption (SEA) and Peak Crushing Force (PCF) performance values, also examined the impact damping values as a result of angular crushing (10°, 20°, 30°, 40°) by changing the crush angles in their crush analysis. According to the results of this research, it was stated that the model with the highest crashworthiness performance was the multi-cell conical model(Qi et al., 2012).

Dağdeviren et al. created crash simulations to observe the resistance of a pickup truck chassis against full frontal and side impacts. The researchers, who handled some parts of the chassis as a preliminary study, carried out axial crush analyzes of square, rectangular and hexagonal cross-section beams with the finite element method. The researchers, who chose the material of the beams as DP600, examined the crush forces of beams with different cross-sections and the energies they absorbed. While the results of the numerical studies were supported by experimental studies, the highest crush force and the highest absorbed energy were observed in the beam with hexagonal section and the chassis modeled with hexagonal parts (Dagdeviren et al., 2016).

In another study, Tarlochan et al. examined the crushing performance of thin-walled structures under axial and angular (30°) loads by numerical crush analysis. Researchers examined the structure with a total of 6 different cross-sections as circular, square, rectangle, hexagonal, octagonal, and elliptical, with 2 different cross-section perimeters and 3 different thicknesses; While using A36 steel as the material, they defined the material with Johnson-Cook material parameters for the finite element method. Then, these structures were filled with aluminum foam and evaluated in terms of crush performance, cost, and ease of production. As a result, thin-walled structures with hexagonal sections showed the best crush performance, ease of manufacturing, and cost. While Tarlochan et al. stated that the energy absorbed by the 2 mm thickness hexagonal tube directly under load was 26 kJ, and the Crush Force Efficiency (CFE) was 0.68; They stated that it absorbs 16 kJ of energy under angular load and the CFE is 0.71. They added to the results that aluminum foam increased these performance values by almost 10% (Tarlochan et al., 2013).

Gao et al. analyzed the elliptical section tube filled with arbitrary foam using the finite element method and compared them with square, rectangular and circular section tubes. AL 6060 T4 aluminum alloy material is used in the models created with different loading angles. Researchers validated their numerical studies with experimental data used in different studies. In order to keep the crush performance values obtained at the optimum level, they used a Multiobjective optimization design (MOD) and tried to keep the SEA value the highest and the CFE the lowest in this optimization. Gao et al., who tried to determine the optimal situation by using the radial rate (f), the thickness of the wall (t), and foam density

(ρ_f) parameters, stated that the structures showed better collision performance in cases where these values were higher(Gao et al., 2016).

Brown et al. examined an elliptical cross-section crush box by creating a collision simulation. Researchers used the ANSYS program for crushing simulation. Researchers using A36 steel as the material in these numerical analyzes confirmed the results of the analysis with the results of another research. Examining crushing performance criteria such as specific energy absorption and crush force efficiency by drilling different numbers of holes in the elliptical cross-section crush box, Brown et al applied the collision loads axially and angularly (5°, 30°). In the results of the research, it was stated that the drilled holes increase the energy absorption and decrease the CFE value (Brown et al., 2020).

Dhaneesh et al. stated that the distance between the impact and the passenger is very low in the event of a side impact and investigated the impact strength of an automobile door using the finite element method. Focusing on the strength of the impact beams inside the vehicle door, the researchers compared the C-section impact beam in the vehicles with the newly designed M-type beam. Dhaneesh et al., who made their analysis in the LS-Dyna program, used Docol 1200 steel as the material. The researchers stated that according to the results of the analysis, 25% less deformation was observed in the new design impact beam and the beam absorbed 40% more energy (Dhaneesh and Prabakaran, 2016).

In another study, Shojaeifard et al. numerically observed their energy absorption abilities by placing a side load on square, circular and elliptical cross-sectional beams. Comparisons of these beams with empty beams were made by including the aluminum foam-filled models of these beams in the research. The wall thicknesses of the beams were determined as 1.5 mm and 2 mm. In the simulation, a wedge-shaped impactor was struck through the center of the beams. Impactor's speed is 8 m/s and its mass is 20 kg. While the length of the beams was determined as 240 mm, the width of the square section beam was determined as 20 mm, the outer diameter of the circular section beam was determined as 24.47, and the diameters of the elliptical section beam were determined as 33.95 mm and 16.97 mm. The material of the beams is determined as Al 6063 T3. This material is defined in the simulation with the Piecewise Linear Plasticity material model. In the simulation, the friction coefficient between the surfaces was determined as μ=0.2 and was entered into the analysis. An analytical examination of this problem is also included in the research. Finally, the results of the analysis were confirmed by the experimental results obtained in another study. According to the results of the research, the elliptical section beam showed the best energy absorption performance among the empty beams (for 1.5 mm: SEA= 1990, Max. peak load=4.38, crash load efficiency= 60%). SEA values in beams filled with aluminum foam are compared to empty beams; For 1.5 mm thick beams, it was observed that it increased 22% in elliptical, 38% in circular, and 18% in a square, while for beams with 2 mm thickness there was an increase of 66% in elliptical and 73% in the circular (Shojaeifard et al., 2012).

Ghadianlou et al. also discussed the impact strength of the beams inside the door. Researchers compared these scenarios using three different materials (Aluminium 3105-H18, Magnesium AZ31B, High Strength Steel A441) and three different thicknesses (1, 1.5, and 2mm). While constraining the beams in the simulation to two rigid walls, they fixed one and defined movement to the other. The researchers, who defined a speed of 10 m/s and weight of 30 kg on this moving wall, observed the SEA values of 6 different scenarios. While it was stated that the increase in wall thickness increased the absorbed energy, they explained that the magnesium alloy met the necessary crash-resistance performances to be used in the automotive industry (Ghadianlou et al., 2012).

Rasooliyazdi et al. aimed to increase the specific energy absorption of the door impact beams and decrease the peak load as a result of a side collision. The researchers used 3 different materials (Steel AISI 1006, Magnesium AZ31B, Aluminum 3105-H18) and investigated the collision performance of the elliptical beam at 3 different axial angles (0°, 45°, 90°). Rasooliyazdi et al., who carried out the research with the finite element method, used the Ls-Dyna program to create the simulation and defined the material properties in the program using the Piecewise-Linear-Plasticity material model. In the simulation, they defined a mass of 10 kg and a velocity of 5 m/s to the rigid wall impinged on the beams and determined the analysis time to be 25 ms. The researchers examined the results with an optimization method, and determined the optimization parameters as the ratio of the large and small diameters of the elliptical section (r=b/a) and the wall thickness of the beam (t), and examined the SEA and Peak Load of the beams. According to these results, the researchers explained the most optimal design as r=0.25/t=2.5 mm and stated the SEA value of this design as 456.9 J/kg and the peak load as 1.4967×10^5 N (Rasooliyazdi et al., 2014).

More et al. investigated the impact resistance of the side door beams in collisions from the side of the vehicle with numerical and experimental analyzes. The researchers performed their analyzes with three different beam section types (Circular, HAT-section, M-section) and three different materials (AISI 1008, BH-220, DP-450). The researchers, who determined the length of the beams as 900 mm, also determined the thicknesses as 1.4 mm, 1.6 mm, and 1.8 mm. The researchers, who carried out the experimental tests on a three-point bending test device and the numerical analyzes with the finite element method, stated that the best results (SEA and Reaction Force) were observed in 1.8 mm thick, m section shape type, and AISI-1008 material (More et al., 2020).

In another study examining the performance of the door beams inside the vehicle door, Krishana et al. analyzed the absorbed energy and reaction force data by giving a certain load to the rectangular and circular section beams. The length of the beams is 370 mm, the square section measures 60x40x1.9mm and the circular section measures 33.8x3 mm. The impactor speed in the experimental test is 2.5mm/min and the impactor speed in the numerical analysis is 2.5mm/ms. Experimental and numerical tests, which are quasi-static, were validated with each other. According to the results, the researchers stated that a rectangular beam has a 34% better energy absorption ability than a circular beam (Krishana et al., 2018).

Nichit et al., experimentally and numerically, analyzed the crash performance of beams inside the vehicle door using four different cross-sections. These cross-sections are C-channel, Square-section, I-section, and Circular-section. The lengths of the beams are determined as 450 mm, but the thickness of the beams is different (I-section=1.1 mm, Circular=2.1mm, C-channel=1.6mm, square=1.3mm). Experimentally, the researchers, who carried out their analyzes using the universal three-point bending device, also created the collision simulations using the Ls-Dyna analysis program. Researchers who use AISI 1010 steel as a material defined the properties of this material in the program. The researchers created a similar model of the test device in the simulation. The punch in the test device is 40 mm and the punch is given a speed of 0.01 m/s. According to the research results; the highest maximum bending force was observed in I-shape as 8.6 kN (Nichit and Battu, 2017).

While there are many studies dealings with side collision scenarios of vehicles, in these scenarios, researchers have generally focused on door support beams. Černiauskas et al. combined 5 different door beam models with 5 different materials as shown in Figure 2.1. A punch with a diameter of 100 mm was used in the created impact simulation and experimental test equipment. This punch moved 150 mm and applied a bending force to the beams with a speed of 2mm/ms. The material of the beams was determined as I-AA6061, II -AISI 1080, III -AISI 1060, IV-AISI-1018, and V-Steel 20 GHOST, respectively, and defined for the simulation. Černiauskas et al., who subjected the samples to the experimental test, created simulations of this test in the Ls-Dyna program and examined the deformations of the samples according to the applied load. As a result, they explained that without common requirements for beam strength, usage of sufficiently rigid closed profile beams of different materials and cross-sections might be unreasonable, and open profile beams possibly do not meet minimal stiffness requirements (Černiauskas, et al., 2010).

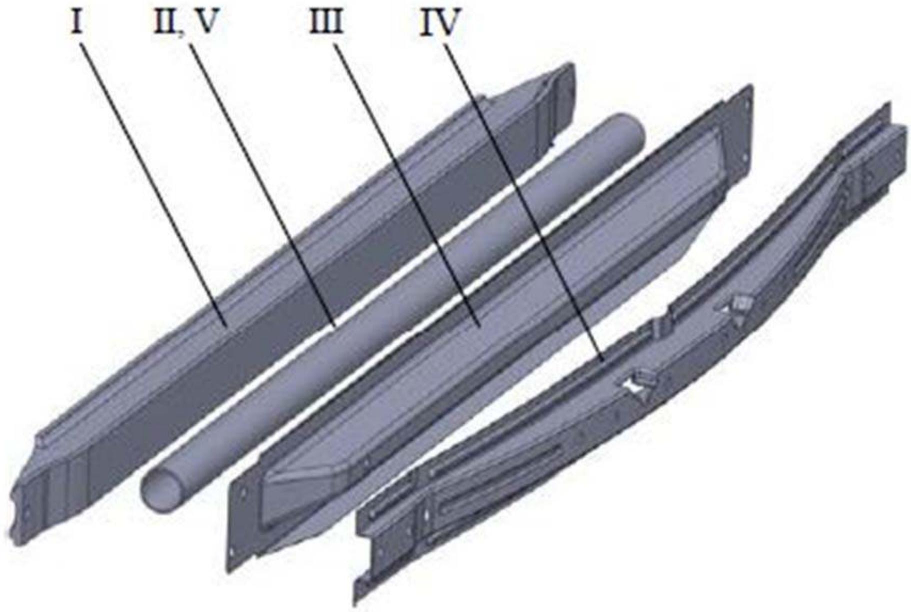

Figure 2.1. Beam models in the work of Černiauskas et al.

Nemani et al. stated that the distance between the impactor object and the driver is small in side impacts and expressed the importance of door beams. For this reason, Nemani et al., who conducted research on door beams, investigated three different types of beam sections experimentally and numerically (M-shape, HAT-shape and Circular cross-section). The researchers determined the length of the beams as 900 mm, the thickness as 2 mm and the material as AISI 1080. While defining different displacement values to the punches in the simulations, they applied loads at different distances from the ends of the beams. The researchers, who processed the obtained values with the Taguchi Method, obtained the results of 27 scenarios without the need to perform all the experiments. According to the results of the research, HAT-shape section beam gave the best SEA value. In addition, the researchers stated that the energy absorption abilities of the beams vary according to the place where the load is applied and displacement of the load (Nemani and Arakerimath, 2015).

Ponnadai, in a comprehensive thesis study, compared the strength properties of 10 different types of beams under load.
These beam models are;

1- Circular cross-section profile beam,
2- I – Type cross-section profile beam,
3- Double L cross-section profile beam,
4- II – Type cross-section profile beam,
5- Circular thick-walled profile beam,
6- III – Type cross-section profile beam,
7- Single rib cross-section profile beam,
8- M – type cross-section profile beam,
9- Square type cross-section profile beam,
10- X–type cross-section profile beam.

The thickness of the circular thick-walled profile beam is 4 mm, and the thickness of all other beams is 2 mm. Researcher determined the materials of the beams as aluminum alloy, cast alloy steel, steel AISI 1060. The researcher, who performed their simulations Static Structural and Explicit in the ANSYS program, defined the properties of the materials with the Bilinear Isotropic Hardening (BISO) plasticity model. The results that the researcher wanted to get from the analyzes were Directional Deformation, Specific Energy Absorption, and Force Reaction. According to these results, when a comparison is made between beam models; for Aluminum Alloy, the lowest directional deformation is seen in the Double L cross-section profile beam, while the best SEA value is seen in the III–

Type cross-section profile beam, for Cast alloy steel the lowest directional deformation is seen in the Double L cross-section profile beam, The best SEA value was seen in II–Type cross-section profile beam and finally, for Steel AISI 1060 material, the lowest directional deformation was observed in M–type cross-section profile beam, while the best SEA value was observed in Square type beam (Ponnadai, 2018).

Ghadianlou et al. created a collision simulation by including the beams inside the vehicle door, this time including the entire vehicle door in the finite element analysis. Unlike the others, crushing analysis was performed at low speed in this study. For this reason, the impactor speed was determined as 4 m/s. In this study, the mass of the pole impactor was determined as 20 kg and the total mass of the door of the vehicle was determined as 6 kg. Researchers examined beams with 5 different materials and selected these materials as Magnesium AZ31B-H24, Aluminum 5050-H32 sheet, Steel wrought 321, Aluminum 6063-O sheet, and Aluminum 2219-T31 sheet. The selected materials were defined in the analysis program using the Piecewise-Linear-Plasticity, material model. While examining the results, Aluminum 5050-H32 sheet and non-aluminum alloy materials were analyzed according to their elastic modulus and aluminum materials were compared according to their yield strength separately. In the other part of the research, the beams were reanalyzed by defining 1mm, 2mm, 3mm and 4mm thicknesses. Finally, adding ribs into the beams and adding a different parameter to the analysis, the researchers explained the results as follows;

- Low young modulus caused low rigidity and high strength materials caused less deformation,
- Increasing the beam thickness decreased the deformation.

- Rectangular-crossover rib shape beams have the highest resistance to collision, besides, better results were obtained with beams placed opposite and parallel to the normal vector direction of impact.
- With the developed beams, the permanent deformation resulting from the collision has been reduced from 3.3 cm to 0.6, by 80%, peak deflection by 36%, and the permanent deformation of energy absorption by 50%.

3. MATERIAL AND METHOD

3.1. Materials

Various materials are used for different purposes in the automotive industry. The most commonly used materials are aluminum and steel alloys. These materials are generally preferred in security parts due to their high energy absorption ability and high strength. Within the scope of this research, the materials of the support beams placed on the door model were determined as Aluminum Alloy 6061-T6 (AL 6061-T6), A36 steel.

3.1.1. Aluminum Alloy 6061-T6

AL-6061-T6 material is one of the most widely used materials in light and robust structures. It has strong mechanical properties, exhibits good weldability, is easy to form, and is widely extruded. It is often preferred in impact energy-absorber structures because of the high energy it absorbs per unit mass. Its cheapness and easy availability are among its other advantages. The chemical content and mechanical properties of AL-6061-T6 are shown in Tables 3.1 and 3.2.(Lesuer et al., 2001)

Table 3.1. Aluminum 6061-T6 chemical composition (ASM, 2022)

Aluminum 6061-T6 Chemical Composition (Wt.%)									
Fe	**Si**	**Cu**	**Mn**	**Mg**	**Zn**	**Cr**	**Ti**	**Others**	**Al**
0.7 (max)	0.4-0.8	0.15-0.4	0.15 (max)	0.8-0.12	0.25 (max)	0.04-0.35	0.15 (max)	0.15 (max)	Remainder

Table 3.2. Aluminum 6061-T6 mechanical features (Kaya and Özyurt, 2022)

Aluminum 6061-T6 Mechanical Features				
Yield Strength (MPa)	**Tensile Strength (MPa)**	**Density (kg/m^3)**	**Elastic Modulus (GPa)**	**Poisson Ratio**
276	562	2700	70	0.33

3.1.2. A36 Steel

A36 is a low-carbon steel. Low carbon steels are classified as having less than 0.3% carbon by weight. This allows A36 steel to be easily machined, welded, and formed making it highly useful as general purpose steel. The low carbon also prevents the heat treatment from having too much effect on the A36 steel. A36 steel usually has small amounts of other alloying elements such as manganese, sulfur, phosphorus, and silicon. These alloying elements are added to A36 steel to give it the desired chemical and mechanical properties. A36 does not have excellent corrosion resistance as it does not contain high amounts of nickel or chromium. However, this material, which has a high collision energy absorption, is used in many areas of the automotive industry, especially in safety elements (Anonymous, n.d.-a). The chemical content and mechanical properties of the material are shown in Tables 3.3 and 3.4.

Table 3.3. A36 chemical composition (Anonymous, n.d.-b)

A36 Chemical Composition (Wt.%)						
Fe	**C**	**Cu**	**Mn**	**P**	**Si**	**S**
98	0.25-0.29	0.20	1.03	0.04	0.28	0.050

Table 3.4. A36 mechanical features (Anonymous, n.d.-c)

A36 Mechanical Features				
Yield Strength (MPa)	**Tensile Strength (MPa)**	**Density (kg/m^3)**	**Elastic Modulus (GPa)**	**Poisson Ratio**
250	400-550	7900	190-210	0.27-0.30

3.2. Methods

3.2.1. Finite Element Method

Engineering problems cannot always be solved theoretically because when every parameter is wanted to be included in the calculations, inextricable equations arise. Researchers and manufacturers use the finite element method to solve such inextricable problems. In the finite element method, the models are divided into many parts and a mesh structure is created on the model. Mathematical calculations are made separately for each part so that the closest results are obtained. As a computational technique used in engineering to obtain approximate solutions to boundary value problems, the FEM(Finite Element Method) solves several hundred or several thousand equations that need to be solved on a computer. With finite element analysis, programs solve many problems by simulating, from fluid flow to heat transfer, from structural analysis to crashing (Ovalı, İ. 1999). The crashing simulation, which is the main theme of this study, has been maden using the Explicit Dynamics module of the ANSYS program, which can perform many simulations using the finite element method.,

3.2.1.1. Explicit and Implicit Analyses

Explicit and implicit methods are used in numerical analysis to reach solutions to ordinary and partial differential equations with time and to obtain numerical approximations that require computer-based simulations of physical processes. Explicit methods calculate the state of the system after a certain time from the instantaneous state, while implicit methods find a solution by solving an equation that includes both the current state of the system and the next state. For all nonlinear and dynamic analyses, the applied forces at the boundary conditions must be applied incrementally. Implicit and explicit methods are often used to solve these problems. In static analysis, there is no mass (inertia) or damping effect. In the dynamic analysis, mass/inertia and damping-related nodal forces are included. Dynamic analysis can be done via explicit solver or implicit solver. In nonlinear implicit analysis, the solution of each step requires solution iterations to balance within a certain tolerance. In the Explicit analysis, no iteration is required as the node accelerations are solved directly.

Implicit and Explicit analyzes differ in the time increment approach. In implicit analysis, each time increment must converge, but you can set quite long time steps. In contrast, Explicit analysis need not converge in every time interval, but time increments must be very small for the solution to be accurate. Implicit transient analysis has no time limit. Implicit time steps are usually larger than explicit time steps.

Both implicit and explicit solvers solve the same kind of problems. Technically both should give the same result for all cases. You can analyze the same problem with both approaches. The only difference is the approach to the time increment. But this approach is vital (Çapar, 2020). The comparison of Explicit and Implicit analyzes is basically shown in the Figure 3.1.

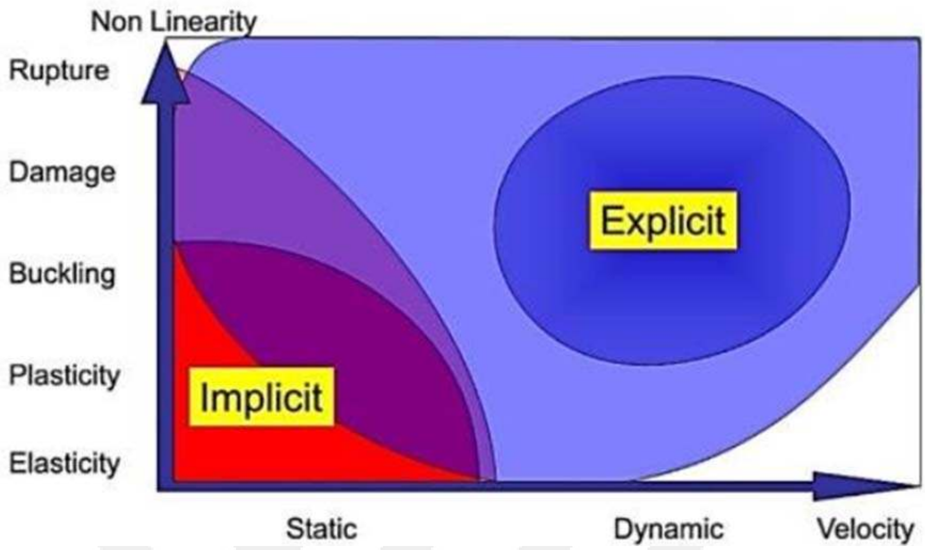

Figure 3.1. The basic comparison of explicit and implicit analyzes(Çapar, 2020)

The explicit method should be used when the strain rate is equal to 10^{-3} per second or more. These events can be illustrated with some examples such as automobile accidents, ballistic explosions, and falls. In such cases, the rate of strain should be considered, as well as the variation of stress with stress.

3.2.2.Material Models

The rate at which the component strains for some materials may have an effect on the results. This is due to the strain-rate sensitivity of the material. The strain rate domain is typically split into 3 categories, namely low or quasi-static strain rates (10^{-5} to 10^{-1} s^{-1}), intermediate strain rates (10^{-1} to 10^{2} s^{-1}), and dynamic strain rates (10^{2} to 10^{4} s^{-1}). Materials loaded quasi-statically typically do not indicate any strain rate sensitivities. It is only in the intermediate or dynamic loading regime that materials appear harder or stronger than they did when loaded quasi-statically. While the stress ratios are very low in tests dealing with the running of people, high dynamic stresses occur in explosions and car accidents. Dietenberger et al. propose five of many different material models for strain and strain-rate hardening in automotive crashworthiness applications (Dietenberger et al., 2005). These 5 models are as follows:

- Piecewise Linear Plasticity Formulation or Multilinear Isotropic Hardening
- Plastic Kinematic Hardening,
- Mixed Piecewise Linear Plasticity with Cowper-Symonds Model,
- Johnson-Cook, and
- Zerilli-Armstrong

3.2.2.1. Piecewise Linear Plasticity/ Multilinear Isotropic Hardening

Of the 5 material models, the piecewise linear formulation is the most widely used in automotive type applications (Simunovic et al., 2003). In this model, the stress-strain curve is made up of discrete data points, which unlike other models, do not first need to be fitted to some predefined equation. Rate effects are accounted for by defining a table of curves at different strain rates. The strain rate is computed in each element of the finite element model and interpolated from the table of curves. If the computed strain rate is outside of the table of curves the value from the nearest available strain rate is used (Long, 2015). This material model is seen with different model names in different programs. It is found under the name Piecewise Linear Plasticity in LS-Dyna program and as Multilinear Isotropic Hardening in Ansys. These material models, which are basically similar, are created with different inputs in each program.

3.2.2.2. Plastic Kinematic Hardening (Cowper-Symonds)

The Cowper-Symonds model serves to incorporate rate effects to other material models which do not already include their own rate dependent parameters. The plastic kinematic hardening model scales the yield stress in accordance with the strain rate as per Equation 3.1. It is best suited for modeling isotropic and kinematic hardening.

$$\sigma_y = \sigma_0 \left[1 + \left(\frac{\dot{\varepsilon}}{C}\right)^{1/p}\right] \tag{3.1}$$

where σ_0 is the initial yield stress, $\dot{\varepsilon}$ is the strain rate; C and P are the Cowper-Symonds strain rate parameters.

3.2.2.3. Mixed Piecewise Linear Plasticity with Cowper-Symonds Model

This material model differs from the piecewise linear plasticity model in that only one set of discrete data points defining a stress-strain curve is used in conjunction with the Cowper-Symonds equation to introduce rate effects. The data set is typically obtained at the lowest strain rate as is practicable with any rate effects introduced as a result of the test being offset by scaling the data. This reduces the number of experiments that must be conducted, provided that there is readily available information about the rate sensitivity of the material in literature.

3.2.2.4. Zerilli-Armstrong Material Model

The Zerilli-Armstrong material model is a rate and temperature sensitive plasticity model. It accounts for strain hardening, strain rate hardening, and thermal softening effects in metals by developing a dislocation-mechanics based constitutive relationship.

$$\sigma = C_1 + C_2 \,.\, e^{(-C_3 + C_4 . ln\dot{\varepsilon}).T} + \left[C_5 \,.\, (\varepsilon^p)^n + C_6\right].\left(\frac{\mu(T)}{\mu(293)}\right) \tag{3.2}$$

where: C_1, C_2, C_3, C_4, C_5, C_6 and n are constants, T is the temperature in degree Kelvin, ε_p is the effective plastic strain and $\dot{\varepsilon}$ is the strain rate and;

$$\left(\frac{\mu(T)}{\mu(293)}\right) B_1 + B_2.T + B_3.T^2 \tag{3.3}$$

with B_1, B_2 and B_3 being constants. As thermal softening is not regarded $C_6 = B_1 = 1$ and $B_2 = B_3 = 0$.

3.2.2.5. Johnson-Cook Material Model

Johnson and Cook model is a strain-rate and temperature-dependent (adiabatic assumption) visco-plastic material model (Johnson and Cook, 1983). This model is suitable for problems where strain rates vary over a large range, and temperature change due to plastic dissipation causes material softening. The model is expressed in a multiplicative form of strain, strain-rate, and temperature terms. The consequence of the multiplicative form is that the strain-hardening rate at a certain strain will increase when the strain rate increases. Therefore, strain-stress curves for increasing strain rates will tend to fan out (Liang et al., 1999). The Johnson-Cook model is explained by Equations 3.4 and 3.5.

$$\sigma = \left(A + B\varepsilon_p{}^n\right).\left(1 + C.\ln\frac{\dot{\varepsilon}}{\dot{\varepsilon_0}}\right)\left(1 - (T^*)^n\right) \tag{3.4}$$

$$T^* = \left[\frac{T - T_0}{T_m - T_0}\right] \tag{3.5}$$

The terms represent;

- A is the initial yield stress,
- B is the hardening constant,

- ε_p is the plastic strain,
- n is the strain hardening exponent,
- C is the Strain rate constant,
- m is the thermal softening exponent,
- ε is the strain rate
- ε_0 is the strain rate reference,
- T^* is a coefficient that depends on the ambient temperature, the local temperature, and the melting temperature,
- T_m is the melting temperature
- T_0 ambient temperature

The model presented by Johnson and Cook in the eighties it's relatively simple and is connected by three different parts. The first one presents the relationship between strain and stress. The second part describes the relationship between strain rate and stress. The last one connects stress value with material temperature during plastic deformation Johnson-Cook plasticity model provides an accurate description of plastic strain related to high strain rates, even without considering variations in elastic properties (Ascenção et al., 2021).

3.2.3. Impact Theory and Crashworthiness Indicators

3.2.3.1. Impact Theory and Energy Conversations

Structural impact mechanics deals with the response of any physical structure to large dynamic loads that result in a range of failures such as permanent deformation or damage such as tearing. Structural impact mechanics is a knowledge base used in applications ranging from design to maintenance or accident investigations. The severity of the impact is determined by factors such as the striking velocity, as well as the mass, geometry, and material characteristics of the struck and striking bodies (Oppermann, 2012). Impact algorithms typically make use of the strain energy imparted on the material as a result of an impact between two bodies. The strain energy is a function of the work done on the deformable structure through deformation which is based on the applied load, resulting elongation and distribution of stress, and is obtained by integrating over the volume of each element. The equation defining the strain energy is given in Equation 3.6 (Ghadianlou and Abdullah, 2013).

$$U_e = \frac{1}{2}\int_v \sigma \text{ x } \varepsilon \text{ x } dv = \frac{1}{2}K_{eq}.\delta_{max}^2 \quad (3.6)$$

Where σ, ε, and v equal to stress tensor; strain tensor, and element volume respectively. K_{eq}, an inherent characteristic of a material, is the stiffness of the body relating to deflections (δ) and the resultant forces. In an event of a collision, it is quite important to discriminate two types of impacts. In the perfectly elastic collision, the masses could have different velocities after impact and an insignificant amount of energy is transferred among them. However, objects could receive the same velocity after striking together.

In collisions where plastic deformation occurs, the kinetic energy that existed before the masses collided is only transferred to the endpoint where the deformation occurs and is converted into internal energy due to the deformation. In other words, the initial kinetic energy is equal to the sum of the kinetic energy of the masses after the collision and the internal energy transformed due to deformation. Equation explaining this principle are as in equations 3.7.

$$\frac{1}{2}m_p v_p^2 = \frac{1}{2}(m_p + m_d)v^2 + \frac{1}{2}K_{eq}\delta_{max}^2 \quad (3.7)$$

Here m_p denotes the mass of the impactor, while m_d denotes the mass of the hit object. v_p is the final velocity of the impactor before the collision. Here, the collision of a moving object with a stationary object is discussed because; The simulation covered by this study was designed accordingly. Momentum remains constant before and after the collision. This situation is explained as in equation 3.8.

$$m_p v_p = (m_p + m_d)v \tag{3.8}$$

Momentum and energy conservation after the separation of masses are explained as in equations 3.9 and 3.10.

$$\frac{1}{2}m_p v_p^2 = \frac{1}{2}m_p {v_p'}^2 + \frac{1}{2}m_d {v_d'}^2 \tag{3.9}$$

$$m_p v_p = m_p v_p' + m_d v_d' \tag{3.10}$$

Here, v_p' is the speed of the impacting mass, and v_d' is the velocity of the mass that initially stopped at it before it separates after the collision. Finally, the plastic strain energy for the permanent damage of the standing mass is obtained by subtracting the pre- and post-collision kinetic energy of the striking mass and the initially stationary mass. Equation explaining this principle are as in equations 3.11.

$$E_{plastic} = \frac{1}{2}m_p v_p^2 + \frac{1}{2}m_d v_d^2 - \frac{1}{2}m_p {v_p'}^2 - \frac{1}{2}m_d {v_d'}^2 \tag{3.11}$$

3.2.3.2 Crashworthiness Indicators

To evaluate the energy-absorbance of structures, it is necessary to define the crashworthiness indicators. The parameters for instance energy absorption (EA), SEA, and PCF can efficiently evaluate the crashworthiness of structures. Energy absorption can be calculated as in equation 3.12.

$$EA = \int_0^{\delta} F(\delta) d\delta \qquad (3.12)$$

where F(δ) is the instantaneous crushing force with a function of the displacement δ. SEA indicates the absorbed energy (EA_{total}) per unit mass(M_{total}) of a structure as;

$$SEA = \frac{EA_{total}}{M_{total}} \qquad (3.13)$$

where M_{total} is the structure's total mass. In this case, a higher value indicates the higher energy absorption efficiency of a material.

Peak Crushing Force (PCF) is another important indicator in the design of energy absorption structures to absorb the impact energy in a collision. When impact occurs i.e., automotive, PCF can determine the occupant's survival rate; therefore, several occupant's injuries or even death (Liao et al., 2008) are caused by a large PCF. Meaning of PCF is maximum reaction force. Reaction force is the force that occurs at the support points. The response of these points to impact is parallel to the force that the passenger will feel.

In the event that the object with velocity hits the other object, the hit object may stop while the energy is transferred to the other object, it may combine with the other object and move in the same direction as it had at the beginning, or it may bounce back after hitting it. In these study analyses, the pole impactor bounces back at a certain speed after hitting the beams. This is due to the fastening of the rafters from their ends. With the deformations in the beams, some of the energy is absorbed and the pole impactor bounces back at a low speed. The velocity of the pole impactor drops to 0 at some point and then starts to increase in the opposite direction. This value is called as velocity absorption time (VAT) ($\boldsymbol{t_{v\to 0}}$). The time for this speed to fall to zero is parallel to the time the passenger is exposed to the impact.

3.2.3.3. Simulation Model Combinations

In this study, the pole impactor speed was determined as 32 km/h, as in the Euro NCAP side-to-pole impact standard. The mass of the pole impactor was determined as 20 kg and this value was taken from another study (Ghadianlou and Abdullah, 2013). Another parameter that the study focuses on is the angle between the upper beam and the lower beam. In order to research the behaviour of this angle in the collision, angles of 10°, 20°, and 25° degrees were determined and models were created accordingly. The 3D image of the created simulation model is as in Figure 3.2.

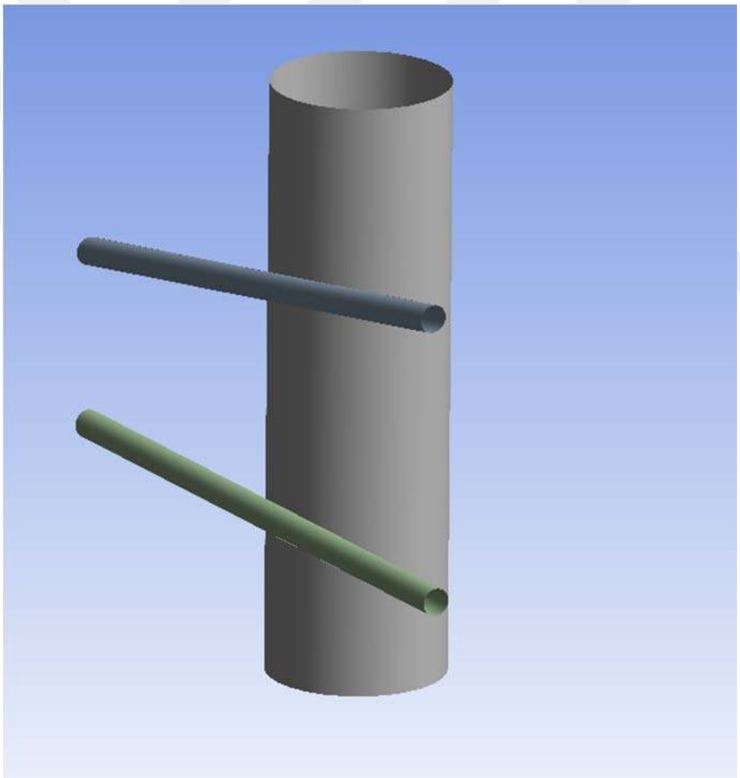

Figure 3.2. Three-dimensional view of the simulation model

Within the scope of the research, beams with 2 different cross-sections, circular and hexagonal, were used and these two different models were compared in terms of absorbed energy. To examine the effect of the beam thickness on the crash performance values, 2 different thicknesses were selected and they are 1.4 mm, and 1.8 mm, respectively. The dimensions of the door support beams were determined in accordance with the beams used in the vehicles. The length of the beams is 900 mm and perimeters of cross-sections of beams is same. The general dimensions of the beams are as in Figure 3.3.

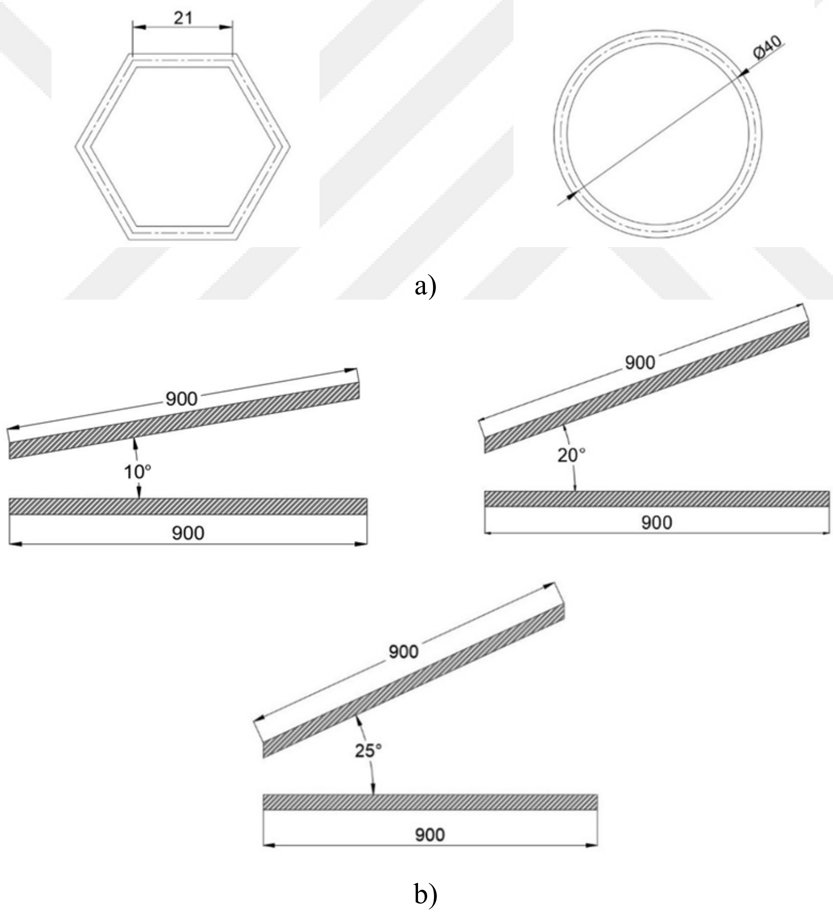

Figure 3.3. Dimensions of beams a) cross-sections of beams b) angles and length of upper and lower beams

3.2.4. Mesh Structure

The meshing of the models was performed with the multizone method as quad/tri elements. As the element size gets smaller, the analysis gives more accurate results, but the analysis time increases significantly. After the mesh convergence study, element size is determined as 5 mm because; while Average Element Quality(AEQ), which is one of the mesh criteria of the ANSYS program, is between 0 and 1 when it is higher than 0.7, it performs the simulation with high accuracy. The AEQ value for the mesh structure applied to the models in this study was over 0.90. Due to simple surface modeling, this value could reach very high values. while the AEQ values of the combinations are shown in Table 3.5, example mesh structure is as shown in Figure 3.4.

Table 3.5. Models mesh qualities

CODES	EQ
10AL14C	0.97262
20AL14C	0.9592
25AL14C	0.9523
10A3614C	0.97262
20A3614C	0.9592
25A3614C	0.9523
10AL18C	0.97262
20AL18C	0.9592
25AL18C	0.9523
10A3618C	0.97262
20A3618C	0.9592
25A3618C	0.9523
10AL14HEX	0.96977
20AL14HEX	0.95727
25AL14HEX	0.95079

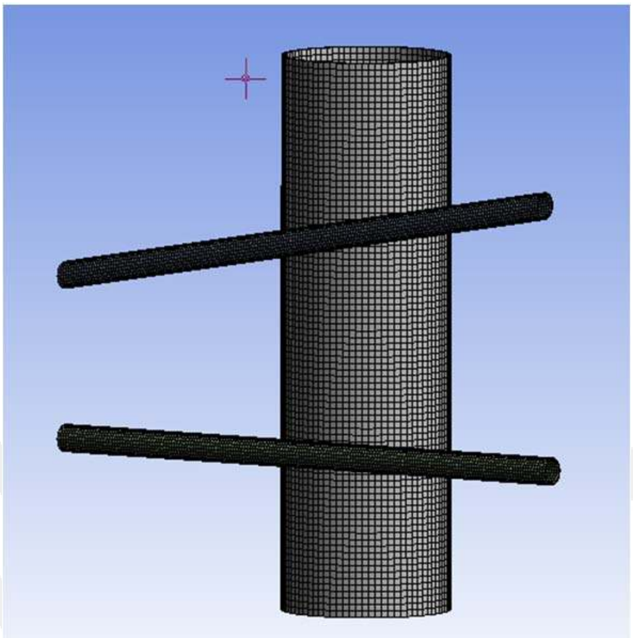

Figure 3.4. The mesh structure of the model

3.2.5. Boundary Conditions

While defining the boundary conditions of the analysis; the beams are fixed at their ends, the material feature is flexible so that the deformation can be observed, and the pole impactor is defined as a rigid material. The movement of the pole impactor is only released in the direction that it will strike the beams, while it is limited in other directions. Frictional contact was assigned to the surfaces of the colliding bodies. The contact between the pole impactor and the rigid wall was set as frictional contact pair with kinematic and dynamic frictional coefficients of 0.2 and 0.1 respectively which is also commonly used in the current literature (Oshinibosi, 2012). The realization time of the simulation was determined as 20 ms because this time is sufficient for the kinetic energy transfer to occur.

3.2.6. Model Validation

Crash performance data were obtained in the simulations performed by applying boundary conditions to the determined combinations. In crashing simulations performed with the finite element method, conservation of energy is considered an indicator of the accuracy of the analysis. Figure 3.5 shows the energy conversation graphic during the crushing process. During the entire impact process, the increase in internal energy is consistent with the decrease in kinetic energy. The total energy of the system is conserved and the sum of the hourglass energy and shear energy is less than 5% of the total energy, proving the reliability of the finite element model (Xu et. al 2021). The accuracy of the analysis is supported by high mesh quality and stable energy transfer.

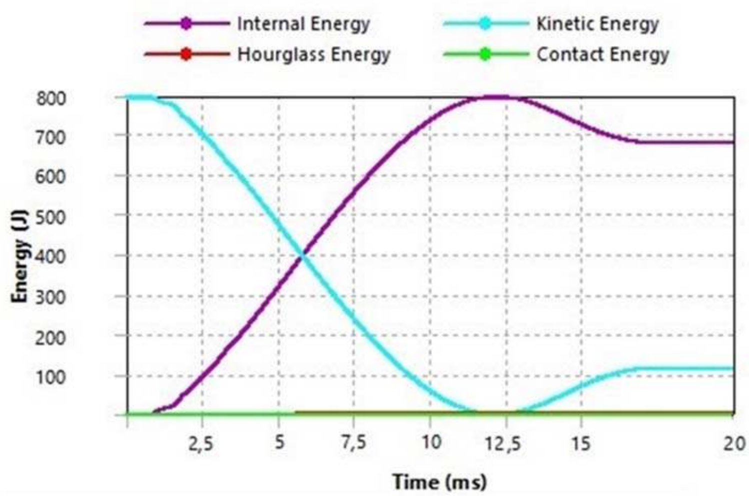

Figure 3.5. Energy change graphic during impact process

It has been calculated that the pole impactor has an energy of 790.125 J thanks to its initial velocity and mass. The energy absorbed by all beam combinations and the kinetic energies of the beams after the bounce were collected and checks were made. It was determined that the biggest deviation in the values was 0.059% and this rate is dependable enough for analyses.

4. RESULTS AND DISCUSSIONS

4.1. Circular Beams

4.1.1. Energy Absorptions Comparison of Beams

After ensuring the reliability of the analyses with mesh studies, the energy values absorbed by the circular cross-section beam combinations were evaluated. These values are as shown with masses of beams in Table 4.1.

Table 4.1. Energy absorption and masses of circular beam combinations

Combinations	Absorbed energy (J)	Total mass (kg)	Combinations	Absorbed energy (J)	Total mass (kg)
10AL14C	674.56	0.8498	10AL18C	664.23	1.0927
20AL14C	675.36	0.8403	20AL18C	665.53	1.0804
25AL14C	675.96	0.8330	25AL18C	665.79	1.0711
10A3614C	743.21	2.4709	10A3618C	740.63	3.1769
20A3614C	743.46	2.4430	20A3618C	740.88	3.1410
25A3614C	743.80	2.4220	25A3618C	741.15	3.1140

According to the results of the analysis, it was observed that the beams defined in A36 steel absorb more impact energy than those defined in AL6061-T6. The highest energy absorption was obtained from the 25A3614C combination with a value of 743.8 J, while the 10AL18C combination with the lowest absorbed 664.23 J. In general, steels show higher strength than aluminum alloys. It is an expected result that A36 steel undergoes less deformation and absorbs more energy than AL6061-T6 material. According to the analysis results, A36 absorbs more energy but, contrary to what is thought, while AL6061-T6 material shows higher peak deformation, it less plastic deformation because it is more elastic. On the other hand, increasing the beam thickness decreased the energy absorbed. Considering Eq. 3.6, it is expected that the energy absorbed will increase due to the increase in deformation. It has been observed that the increase in the angle between the beams slightly increases the amount of energy absorbed, but it is thought that this energy difference may increase to significant levels at higher speeds.

4.1.2. SEA Comparison of Beams

In the automotive field, the lightening of vehicles not only provides low fuel consumption and emissions but also facilitates the portability of vehicles. However, heavy materials may be required due to the need for high material strength to ensure passenger safety in vehicles. AL6061-T6 material is lighter than A36 steel but has lower strength. Nevertheless, having high strength is not the same as exhibiting more energy absorption performance. The comparison of SEA values obtained from the collision simulations of these two materials is shown in Figure 4.1.

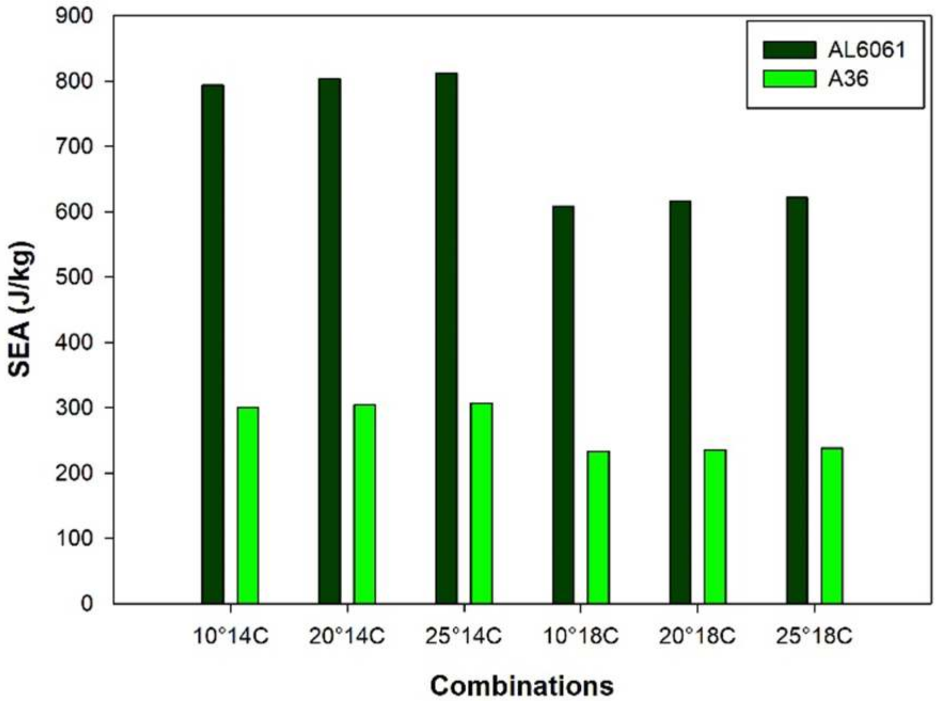

Figure 4.1. SEA comparison according to beam thicknesses and angles

When the results are examined by considering Table 4.1 and Figure 4.1; the beams for which the A36 material is defined have absorbed more energy, but they are heavier. Therefore, beams defined as AL6061-T6 material had higher SEA values. Increasing the beam thickness decreases the SEA value. This is because the increase in mass and the increase in thickness reduce the deformation. Therefore, thick beams have lower SEA, although they absorb higher energy. Increasing the beam angles also increased the SEA as it slightly increased the absorbed energy. Among the beams, the highest SEA value was observed in the combination of 25AL14 with 811.48 J/kg, while the lowest SEA value was obtained in the combination 10A3618 with 233.13 J/kg.

4.1.3. Deformation Comparison of Beams

In crash energy absorber structures, deformation is a parameter that directly affects the absorbed energy. The demand for more or less deformation may vary according to the needs. For the sake of example, increasing the deformation will provide positive results so that the passenger is less affected by the collision under the same loads, but it will increase the maintenance cost. Ductility is also important in deformation results. Ductile materials can get close to their original state after the impact of the impact, that is, their plastic deformations are less. For this reason, plastic deformations are considered together with peak deformations in the structures within the scope of the study. The deformation data of the collision analysis are shown in Figure 4.2.

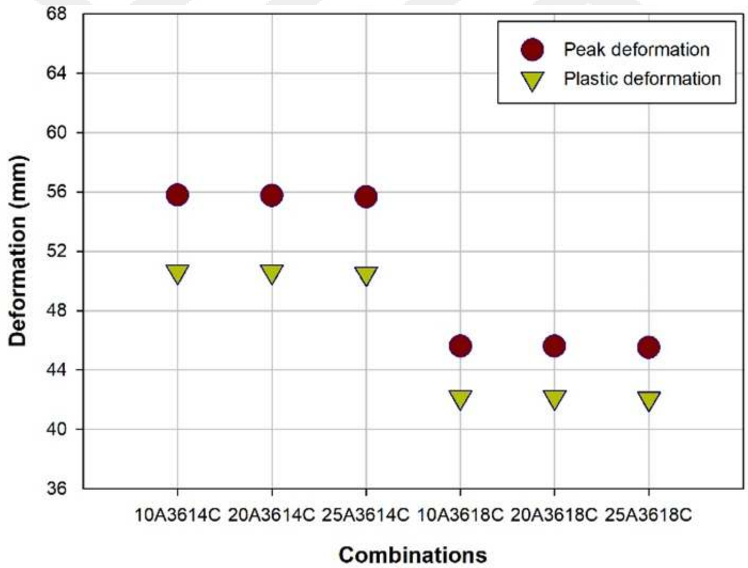

a)

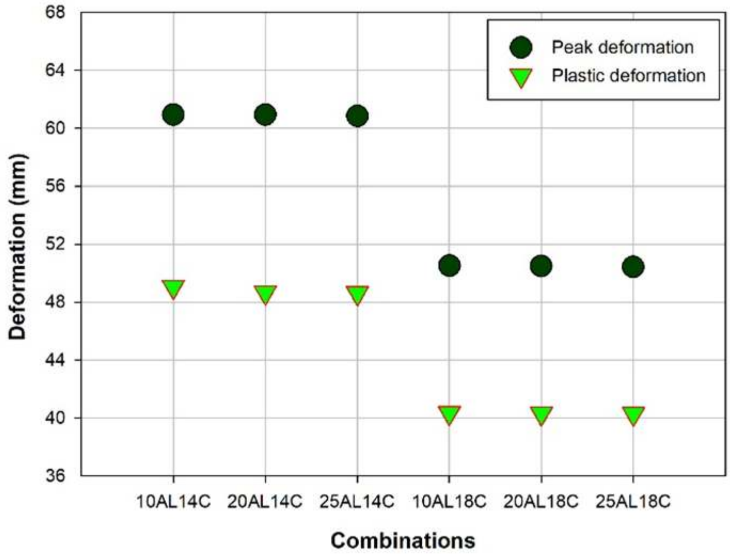
Peak deformation
Plastic deformation
Deformation (mm)
Combinations
10AL14C
20AL14C
25AL14C
10AL18C
20AL18C
25AL18C

b)

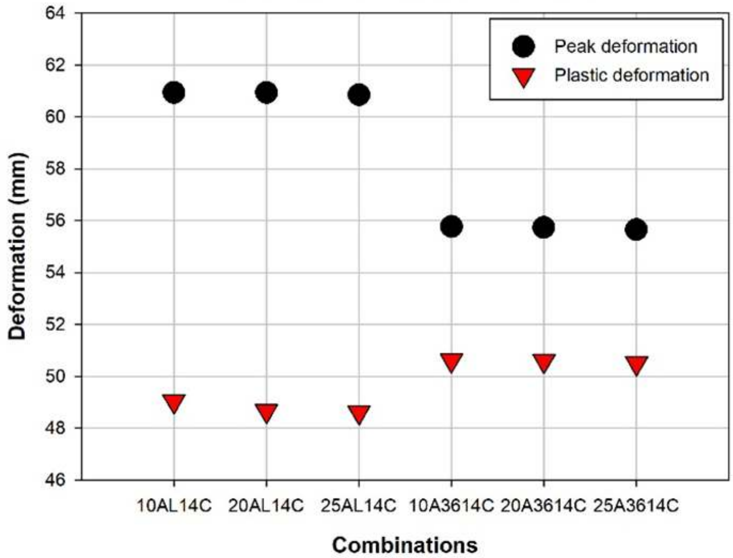
Peak deformation
Plastic deformation
Deformation (mm)
Combinations
10AL14C
20AL14C
25AL14C
10A3614C
20A3614C
25A3614C

c)

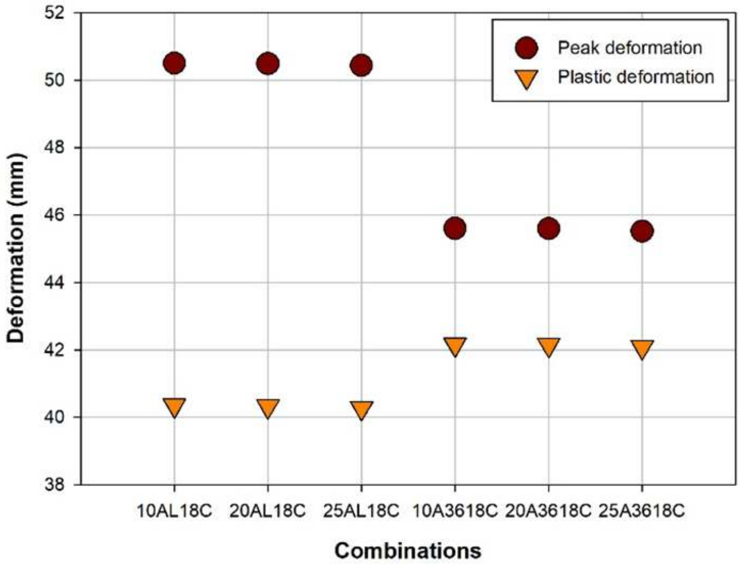

d)

Figure 4.2. Peak and plastic deformations of beams a) A36 b) AL6061-T6 c) 1.4mm thickness d) 1.8mm thickness

When the graphics are evaluated; the highest peak deformation was observed in the combination 10AL14C with 60.93 mm, and the lowest with 45.52 mm in 25A3618. In plastic deformation, the lowest value was found at 25AL18C with 40.27 mm, while the highest value was found in the combination of 10A3614C. While the peak deformation of AL6061-T6 material is higher, the plastic deformation of A36 is higher. This explains why the A36 material absorbs more energy. While the difference between peak and plastic deformations of A36 beams is around 3-5 mm, this difference increases to 9-10 mm in AL6061-T6. The difference between peak and plastic deformation of the defined beams of AL6061-T6 material is related to its ductility and flexibility. In this way, AL6061-T6 can provide maintenance at less cost with less permanent deformation. Increasing the thickness decreased the plastic deformation and accordingly the energy absorbed decreased. The increase in thickness may reduce the maintenance cost, but the increase in the production cost will increase at a similar rate. With the increase in the angle between the beams, the amount of deformation decreased slightly and regularly, but this is at a negligible level. If it is necessary to evaluate that the absorbed energy slightly increases with the increase of the beam angle, it is necessary to accept that the deformation occurs and spreads in different directions.

4.1.4. Reaction Force Comparison of Beams

The resistance of the shock absorbing structures against the load during the collision is important for the passenger to feel the impact force. The high peak value means that the passenger will feel the impact force more. Therefore, it is desirable that this value is not high. In this study, reaction force values were taken according to fixed support. The reaction force values of the collision simulations are as shown in Figure 4.3.

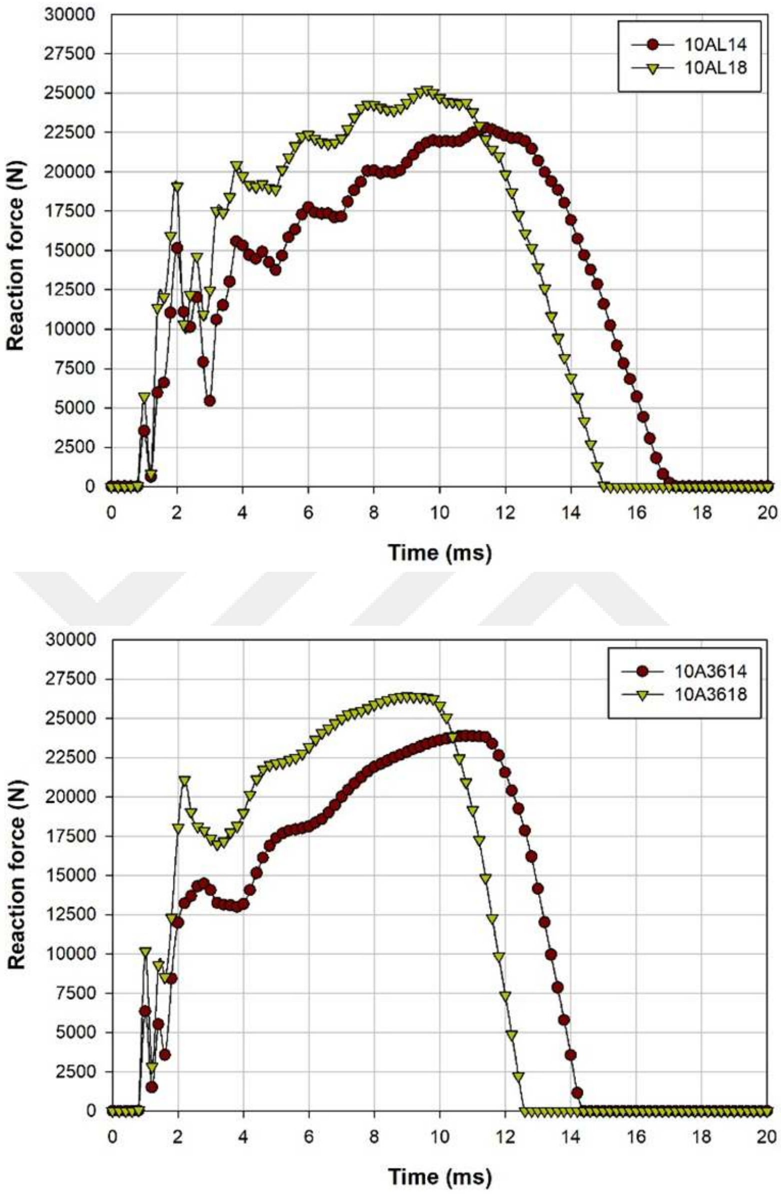
10AL14
10AL18
Reaction force (N)
Time (ms)
10A3614
10A3618
Reaction force (N)
Time (ms)

a)

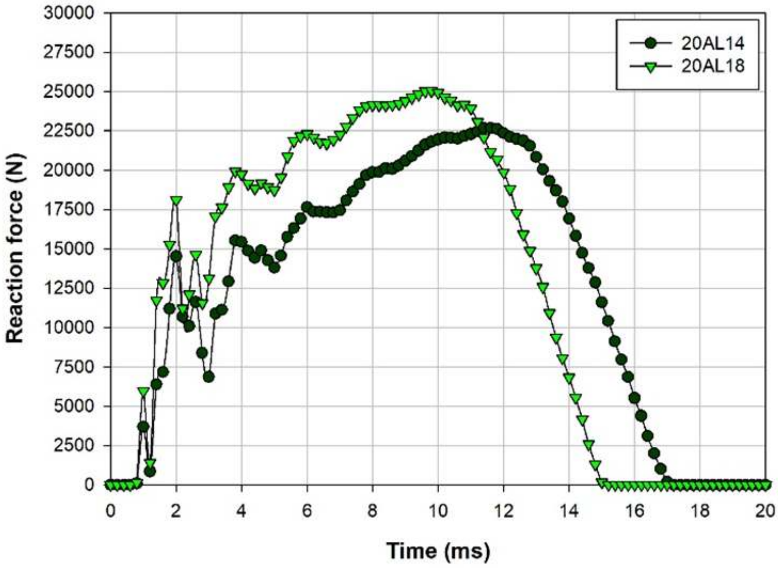

20AL14
20AL18
Reaction force (N)
Time (ms)

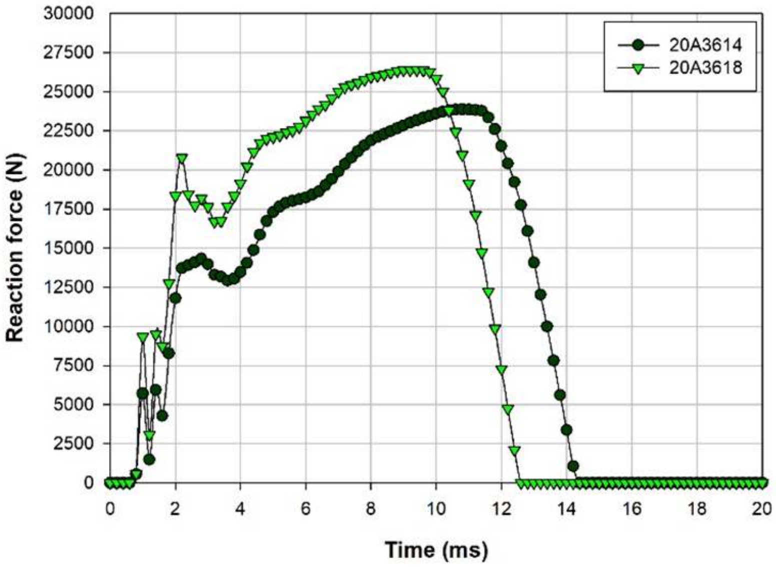

20A3614
20A3618
Reaction force (N)
Time (ms)

b)

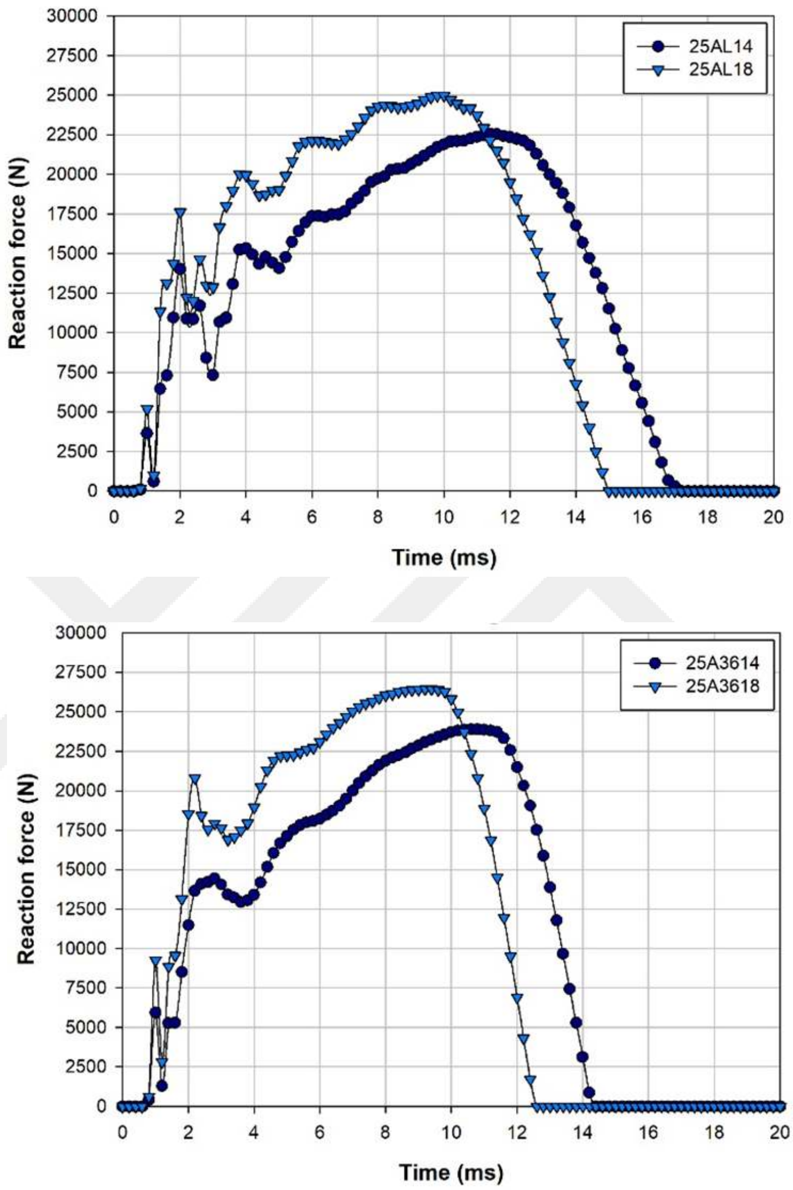

c)

Figure 4.3. Reaction force values a) 10° b) 20° c) 25°

According to the results, A36 material exhibited more reaction forces independently from the thickness and beam angle. Among the combinations, the highest reaction force showed 25A3618C with a value of 26,437 kN. The lowest reaction force was seen at 25AL14C with a value of 22.55 kN. While the reaction force decreased in AL6061-T6 material with an increase in angle, a reverse progression was observed in A36, but this regression is negligible. Finally, it was observed that the maximum reaction force occurred approximately 3-3.5 ms earlier in thicker beams. This could been associated with velocity absorption.

4.1.5. Velocity Absorption Time

Velocity absorption time, called the impactor velocity reduction time to zero, is a measure of the occupant's exposure to force. Even if the collision occurs in a very short time, this value is important for the passenger. The comparison of these values obtained for the combinations in the simulations is performed in Figure 4.4.

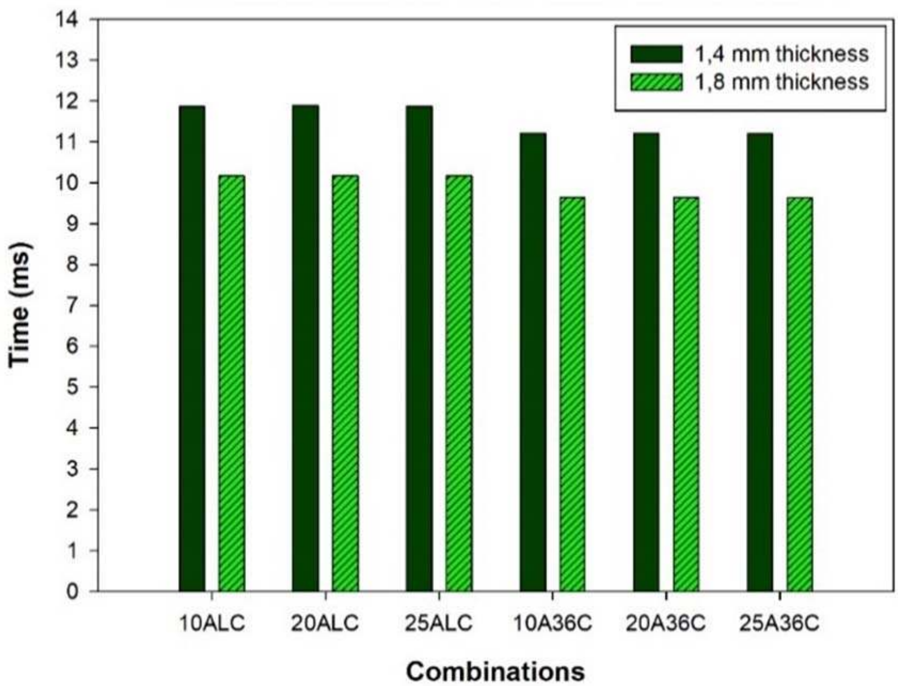

Figure 4.4. Velocity time absorption values

A36 defined beams outperformed AL6061-T6 beams by having lower VAT. The increase in thickness was another parameter that decreased this value. This value increases at 20° beam angles, but beams with 10° beam angles have more VAT than beams with 25° beam angles. According to the results, the lowest VAT value was observed with 9.62 ms in 25A3618C, while the highest value was found in the combination of 20AL14C with 11.88 ms.

4.1.6. Beam Cross-sections

In the last part of the study, the analyses of hexagonal beams are performed and compared with circular beams. Aluminum was defined as the material for both beams and the thickness was kept constant at 1.4 mm. For comparison, the energy absorption and SEA values of hexagonal beams are given in Table 4.2 with circular beams.

Table 4.2. Hexagonal beams energy absorption and SEA values with circular beams

Codes	Absorbed energy (J)	Mass of two beams (kg)	SEA (J/kg)	Peak Deformation (mm)	Plastic Deformation (mm)	VAT (ms)	Reaction Force (N)
10AL14C	674.56	0.850	793.786	60.93	49.044	11.865	22797
20AL14C	675.36	0.840	803.713	60.929	48.658	11.88	22667
25AL14C	675.96	0.833	811.476	60.844	48.615	11.856	22546
10AL14HEX	676.74	0.854	793.794	60.335	49.404	11.9943	22696
20AL14HEX	677.19	0.844	803.086	60.279	49.372	11.9953	22640
25AL14HEX	678.82	0.837	811.754	60.137	49.236	11.9798	22588

According to the results, hexagonal beams have superiority in energy absorption over circular beams, but this advantage is around 1-2 J. Since hexagonal beams have slightly more mass than circular beams due to their geometry, it is seen that they have close SEA values despite their higher energy absorption. When hexagonal beams are compared with circular beams in terms of deformation, more plastic deformation was observed despite less peak deformation. This information explains why hexagonal beams absorb more energy. Deformation images of hexagonal (20AL14H) and circular(20AL14C) beams are shown in Figure 4.5 as example.

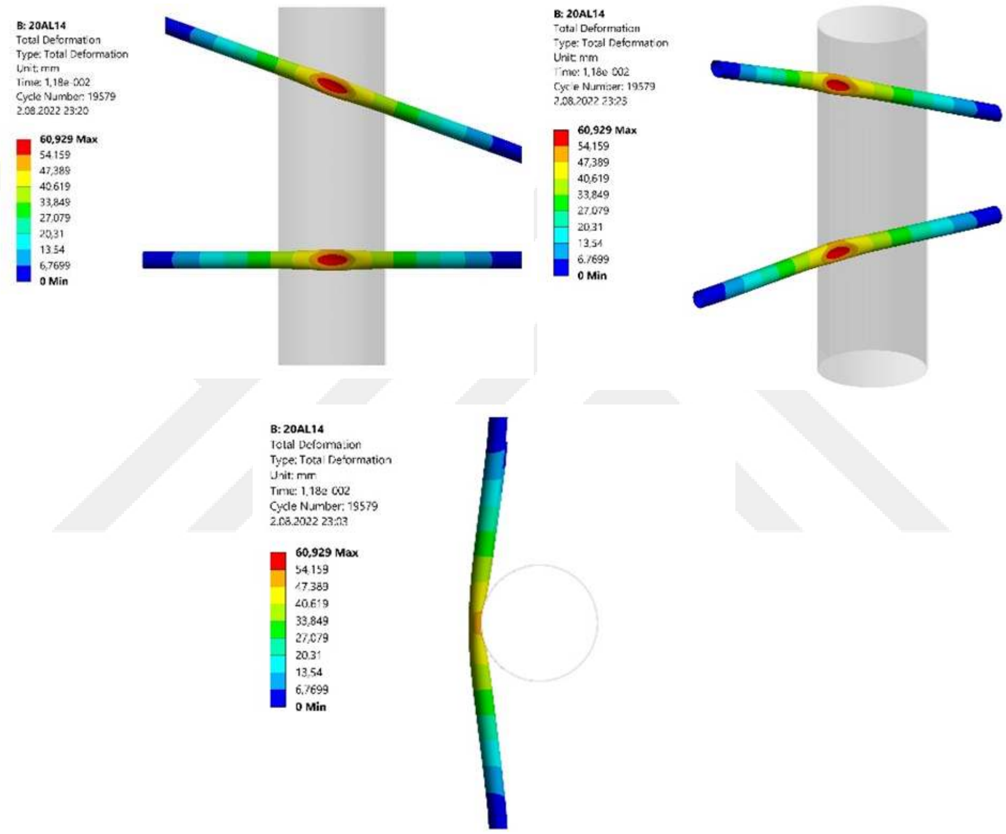

a)

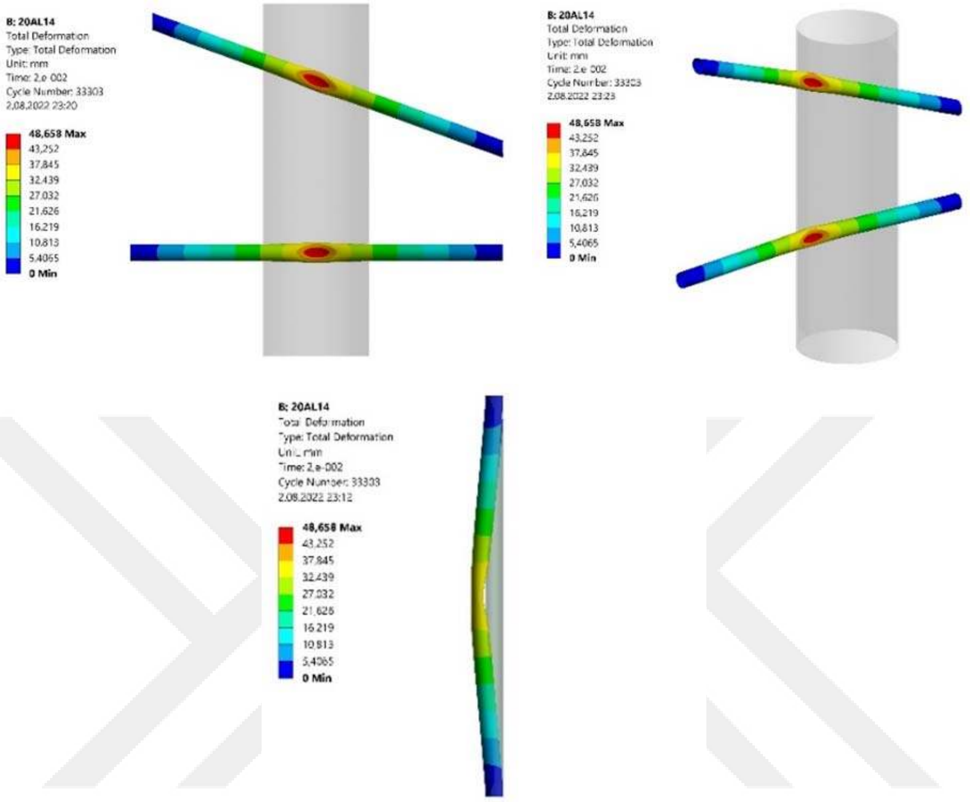
B: 20AL14
Total Deformation
Type: Total Deformation
Unit: mm
Time: 2,e-002
Cycle Number: 33303
2.08.2022 23:20
48,658 Max
43,252
37,845
32,439
27,032
21,626
16,219
10,813
5,4065
0 Min
B: 20AL14
Total Deformation
Type: Total Deformation
Unit: mm
Time: 2,e-002
Cycle Number: 33303
2.08.2022 23:23
48,658 Max
43,252
37,845
32,439
27,032
21,626
16,219
10,813
5,4065
0 Min
B: 20AL14
Total Deformation
Type: Total Deformation
Unit: mm
Time: 2,e-002
Cycle Number: 33303
2.08.2022 23:12
48,658 Max
43,252
37,845
32,439
27,032
21,626
16,219
10,813
5,4065
0 Min

b)

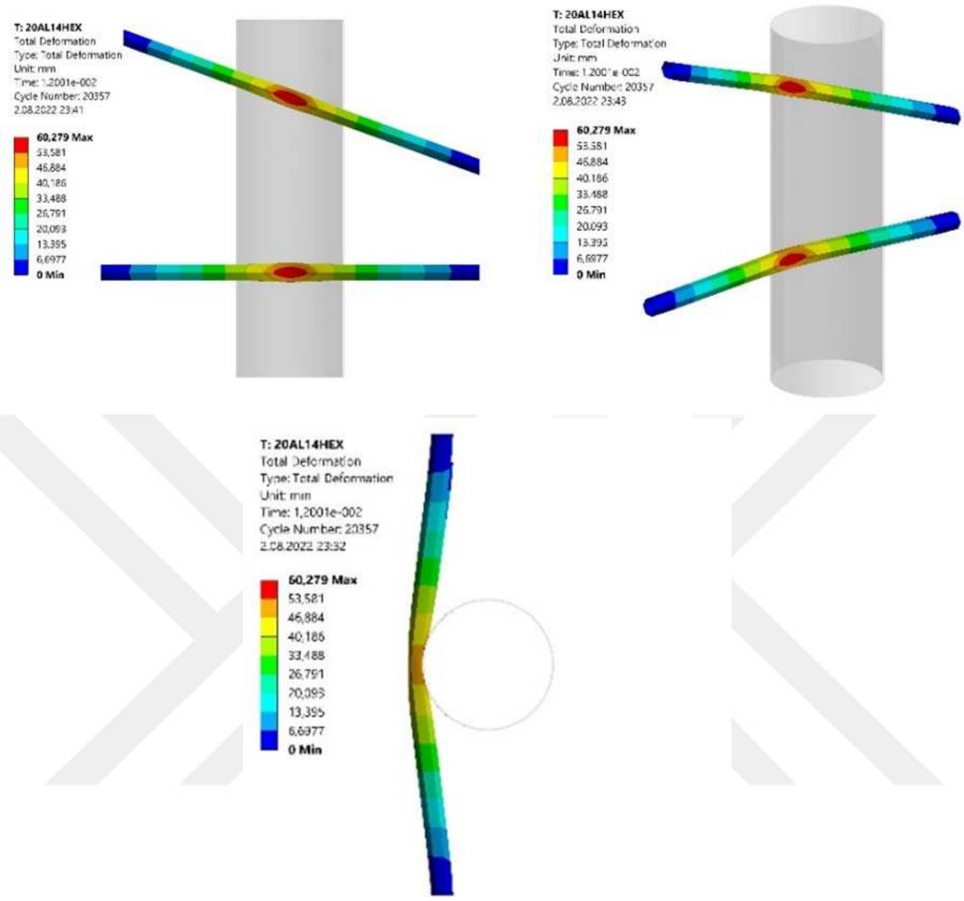
T: 20AL14HEX
Total Deformation
Type: Total Deformation
Unit: mm
Time: 1,2001e-002
Cycle Number: 20357
2.08.2022 23:41
60,279 Max
53,581
46,884
40,186
33,488
26,791
20,093
13,395
6,6977
0 Min
T: 20AL14HEX
Total Deformation
Type: Total Deformation
Unit: mm
Time: 1,2001e-002
Cycle Number: 20357
2.08.2022 23:43
60,279 Max
53,581
46,884
40,186
33,488
26,791
20,093
13,395
6,6977
0 Min
T: 20AL14HEX
Total Deformation
Type: Total Deformation
Unit: mm
Time: 1,2001e-002
Cycle Number: 20357
2.08.2022 23:32
60,279 Max
53,581
46,884
40,186
33,488
26,791
20,093
13,395
6,6977
0 Min

c)

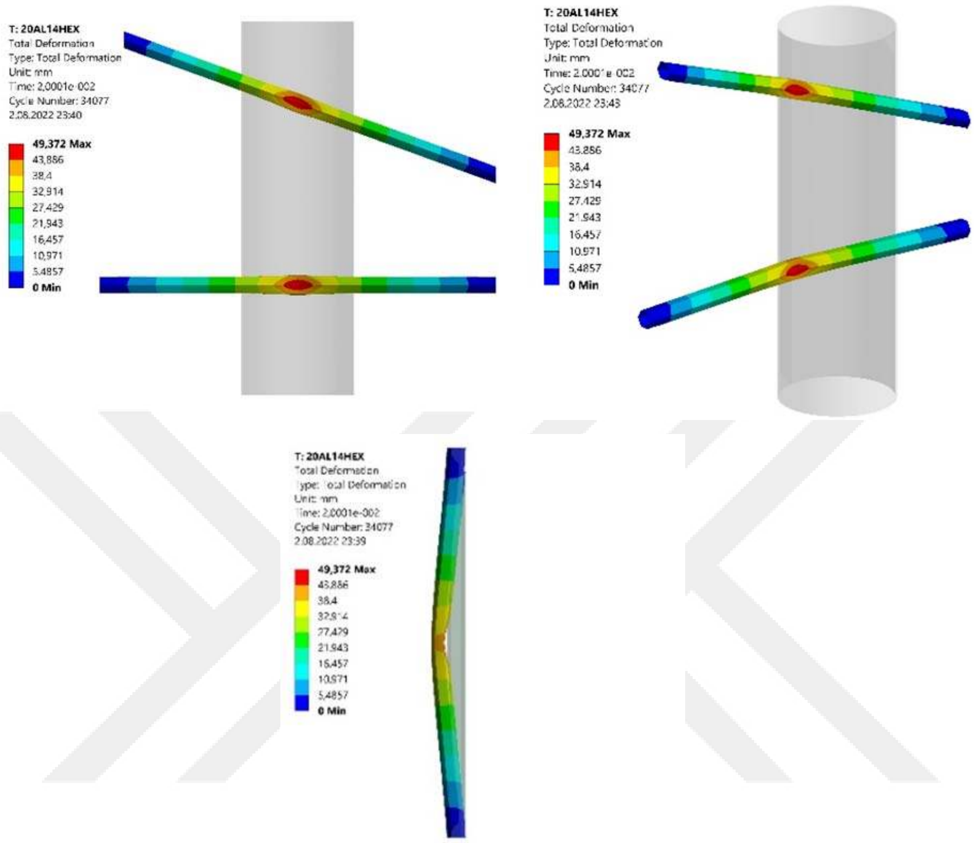

d)

Figure 4.5. Deformation images of beams a) Peak deformation of 20AL14C b) Plastic deformation of 20AL14C c) Peak deformation of 20AL14H d) Plastic deformation of 20AL14H

As with circular beams, the increase in angle increased the reaction force, but the reaction force value of hexagonal beams was lower than that of circular beams. Finally, it has been observed that hexagonal beams reduce the velocity to zero in a longer time. This situation can be shown as one of the disadvantages of hexagonal beams, which give better results than circular sections.

5. CONCLUSIONS

In vehicle accidents that occur with a side impact, the distance between the striking and the passenger is very small. That's why beams in automobile doors are vital for the safety of passengers to absorb impact. The energy absorption and reaction force characteristics of the beams represent the behavior of the beams at the time of the collision. In this study, the energy absorption performances of circular cross-section beams used by many automobile manufacturers were investigated using 2 different materials, 3 different beam angles, and 2 different beam thicknesses. Then, keeping these variables constant, hexagonal beams were analyzed and compared with circular beams. According to the results of the study;

- AL6061-T6 material showed better energy absorption performance with less mass. It deforms better and absorbs more energy.
- VAT value of A36 steel is low than Aluminum 6061-T6. By using this material, passengers will be exposed to impact for less time. However, it should not be forgotten that its energy absorption ability is lower than 6061-T6.
- Since AL6061-T6 is a more ductile material, it has undergone less permanent deformation.
- The increase in thickness reduces the deformation. Therefore, it reduces energy absorption. Due to the increase in mass, the SEA value also decreased. Increasing the reaction force is also one of the disadvantages of increasing the thickness.
- The increase in beam angles has increased the energy absorption values, but this increase is not very large. The lowest reaction force was at the highest angle. Deformation values decreased at a neglectable level.

- Hexagonal beams showed superior energy absorption performance than circular beams. These beams are recommended to automobile manufacturers instead of circular cross-section beams

In this study, which examines the life-saving performance of door beams, the importance of these parts, which are used as passive safety systems, is better understood. The potential for use of different models was demonstrated while observing how geometry, material, and thickness changes affect their energy-absorbing abilities.

REFERENCES

ACEA, 2021. *ACEA Report 2021 Vehicles in Use Europe*. Retrieved from https://www.acea.auto/files/report-vehicles-in-use-europe-january-2021-1.pdf

Anonymous, (n.d.-a) Goodkitchen. Retrieved from https://celik.family.blog/a36-celik/

Anonymous, (n.d.-b) No Title. Retrieved from http://tr.shew-esteelpipe.com/steel-plate-coil/astm-a36-carbon-steel-plate.html

Anonymous, (n.d.-c) No Title. Retrieved from https://tr.goodkitchendesign.com/what-is-a36-steel_14687

Ascenção, F. A., Silveira, M. E., and Pockszevnicki, B. C., 2021. Evaluation of the Effects of the Forming Process on the Simulation of a Crash Test of an Automotive Bumper. SAE Technical Papers, 7.

ASM., (n.d.). Retrieved from https://asm.matweb.com/search/SpecificMaterial.asp?bassnum=ma6061t6

Brown, J. J., Bin Ismail, A.-E., Kidau, D., and Mong, W. C., 2020. Simulation Study of Elliptical Thin Walled Structure Crash Box with Holed Initiator through Axial and Oblique Impact. International Journal of Emerging Trends in Engineering Research, 8(8):4084–4090.

Çapar, Y., 2020. Yasin Çapar. Retrieved from https://yasincapar.com/tr/sonlu-elemanlar-yontemde-implicit-vs-explicit-yaklasimi/

Černiauskas, E., Keršys, A., Lukoševičius, V., and Sapragonas, J., 2010. Investigation of Anti-Intrusion Beams in Vehicle Side Doors. Mechanika, 86(6):11–16.

Dagdeviren, S., Yavuz, M., Kocabas, M. O., Unsal, E., and Esat, V., 2016. Structural Crashworthiness Analysis of a Ladder Frame Chassis Subjected to Full Frontal and Pole Side Impacts. International Journal of Crashworthiness, 21(5):1–17.

Dhaneesh, K. P., and Prabakaran, B., 2016. Study And Advanced Concept For Side Impact Protection Beams To Reduce The Injury Of The Occupant Using CAE. International Journal of Mechanical and Production Engineering, 4(5):55–60. Retrieved from http://www.iraj.in/www.iraj.in › journal

Dietenberger, M., Buyuk, M., and Kan, C.-D., 2005. Development of a High Strain-Rate Dependent Vehicle Model. LS-Dyna Anwenderforum. Retrieved from http://roadsafellc.com/NCHRP22-24/Literature/Papers/Development of a high strain-rate dependent vehicle model.pdf

Ellway, J. D., van Ratingen, M., Goutas, P., Gay, P., Versmissen, T., van Montfort, S., … Ogihara, T., 2013. The Advanced European Mobile Deformable Barrier Specification for Use in Euro NCAP Side Impact Testing. The 23rd ESV Conference Proceedings. Retrieved from http://www-esv.nhtsa.dot.gov/Proceedings/23/isv7/main.htm

Euro NCAP, 2020.a *European New Car Assessment Programme (Euro NCAP) Oblique Pole Side Impact Testing Protocol For 2020 Implementation* (Vol. November).

Euro NCAP, 2020.b *European New Car Assessment Programme (Euro NCAP) Side Impact Mobile Deformable Barrier Testing Protocol* (Vol. June). Retrieved from https://cdn.euroncap.com/media/58234/euro-ncap-side-protocol-ae-mdb-v812.pdf

Euro NCAP, 2021.a How to Read the Stars. Retrieved from https://www.euroncap.com/en/about-euro-ncap/how-to-read-the-stars/

Euro NCAP, 2021.b Vehicle-Safety/the-Ratings-Explained/Adult-Occupant-Protection. Retrieved from https://www.euroncap.com/en/vehicle-safety/the-ratings-explained/adult-occupant-protection/

Gao, Q., Wang, L., Wang, Y., and Wang, C., 2016. Crushing Analysis and Multiobjective Crashworthiness Optimization of Foam-Filled Ellipse Tubes under Oblique Impact Loading. Thin-Walled Structures, 100105–112.

Gaylor, L. M., 2013. *Efficacy of the Thoracic Side Airbag and Effective Occupant Protection in Lateral Impacts*. RMIT University.

Ghadianlou, A., and Abdullah, S. Bin, 2013. Crashworthiness Design of Vehicle Side Door Beams under Low-Speed Pole Side Impacts. Thin-Walled Structures, 6725–33.

Ghadianlou, A., Rasooliyazdi, E., Abdullah, S., Zahari, R., and Farhaninejad, A., 2012. Crashworthiness Evaluation of Vehicle Side Door Beam by Material Investigation and Geometry Modification in Side Impacts. In *Proceedings of the International Conference on Mechanical Engineering and Mechatronics* (pp. 1–6). Ottawa, Ontario, Canada. Retrieved from http://www.academia.edu/4792818/Crashworthiness_evaluation_of_vehicle_side_door_beam_by_material_investigation_and_geometry_modification_in_side_impacts

Hyundai Azera, 2015. Boron Extrication. Retrieved from http://www.boronextrication.com/2009/09/16/hyundai-azera-side-impact-beams-andairbags/

Johnson, G. R., and Cook, W. H., 1983. A Constitutive Model and Data for Metals Subjected to Large Strains, High Strain Rates, and High Temperatures. In *Proceedings 7th International Symposium on Ballistics* (pp. 541–547).

Kaya, D., and Özyurt, E., 2022. Design and Optimization of Impact Attenuator for a Formula SAE Racing Car. Sigma Journal of Engineering and Natural Sciences – Sigma Mühendislik ve Fen Bilimleri Dergisi, 40(2):390–401.

Krishana, R., Yadav, S., Kumar, R., and Paliwal, H. K., 2018. Development and Analysis of Side Door Intrusion Beam of SUV. International Journal of Mechanical Engineering and Technology, 9(9):915–922.

Lesuer, D. R., Kay, G. J., and LeBlanc, M. M., 2001. Modeling Large Strain, High Rate Deformation in Metals. Proceedings of the TMS Fall Meeting, 75–86.

Li, Z., Yu, Q., Zhao, X., Yu, M., Shi, P., and Yan, C., 2017. Crashworthiness and Lightweight Optimization to Applied Multiple Materials and Foam-Filled Front End Structure of Auto-Body. Advances in Mechanical Engineering, 9(8):168781401770280.

Liang, R., Khan, A., 1999. Critical Review of Experimental Results and Constitutive Models for Bcc and Fcc Metals over a Wide Range of Strain-Rates and Temperatures. International Journal o Plasticity, 15(9):963–980.

Liao, X., Li, Q., Yang, X., Li, W., and Zhang, W., 2008. A Two-Stage Multi-Objective Optimisation of Vehicle Crashworthiness under Frontal Impact. International Journal of Crashworthiness, 13(3):279–288.

Liu, M., Guo, Y., Wang, J., and Yergin, M., 2018. Corrosion Avoidance in Lightweight Materials for Automotive Applications. Npj Materials Degradation, 2(1):24.

Long, C. R., 2015. *Analysis of a Car Door Subjected to Side Impact*. University of Cape Town.

Marzbanrad, J., Mehdikhanlo, M., and Saeedi Pour, A., 2009. An Energy Absorption Comparison of Square, Circular, and Elliptic Steel and Aluminum Tubes under Impact Loading. Turkish Journal of Engineering and Environmental Sciences, 33(3):159–166.

Meritor, 2015. Body_Vision Door. Retrieved from http://www.meritor.com/Site Images/Forms/DispForm.aspx?ID=102&RootFolder=%2F%0ASite Images%2F1Body. %0A

More, K. C., Patil, G. M., and Belkhede, A. A., 2020. Design and Analysis of Side Door Intrusion Beam for Automotive Safety. Thin-Walled Structures, 153(May):106788.

Nemani, R., and Arakerimath, R. R., 2015. Taguchi Based Design Optimization of Side Impact Beam for Energy Absorption. Internatıonal Journal for Advance Research in Engıneerıng and Technology, 3(9):100–104.

Nichit, Y. K., and Battu, A. K., 2017. Development of Side Door Intrusion Beam of Passenger Car For Maximum Bending Load. International Journal for Science and Advance Research In Technology, 3(8):1–6.

Oppermann, C. J., 2012. *Study of a simplified bumper system subjected to offset impact loading*. University of Cape Town.

Oshinibosi, A., 2012. *Chassis and Impact Attenuator design for Formula student Race car*. University of Leeds.

Ovalı, İ., 1999. *Ansys Workbench*. Ankara.

Ponnadai, S., 2018. *Analysis of Side Impact Beams in Car Side Door Kaunas University of Technology*. Kaunas University of Technology Faculty.

Qi, C., Yang, S., and Dong, F., 2012. Crushing Analysis and Multiobjective Crashworthiness Optimization of Tapered Square Tubes under Oblique Impact Loading. Thin-Walled Structures, 59103–119.

Rasooliyazdi, E., Zahari, R. Bin, Ghadianlou, A., Farhaninejad, A., Sahari, B. Bin, Aziz, F. A., and Jamali, H., 2014. Crashworthiness Design of Vehicle Side Door Beam Based on Elliptical Geometry Modification Using Multi-Objective Optimization. International Review of Mechanical Engineering (IREME), 8(1):28.

Sharma, N., 2018. *Comparison of Cross sectional Profiles for Side Impact Crash Structure in Passenger Vehicle*. The University of Texas at Arlington.

Shojaeifard, M. H., Zarei, H. R., Talebitooti, R., and Mehdikhanlo, M., 2012. Bending Behavior of Empty and Foam-Filled Aluminum Tubes with Different Cross-Sections. Acta Mechanica Solida Sinica, 25(6):616–626.

Simunovic, S., Nukala, P. K. V. V., Fekete, J., Meuleman, D., and Milititsky, M., 2003. Modeling of Strain Rate Effects in Automotive Impact. Journal of Materials and Manufacturing, 112733–743.

Tarlochan, F., Samer, F., Hamouda, A. M. S., Ramesh, S., and Khalid, K., 2013. Design of Thin Wall Structures for Energy Absorption Applications: Enhancement of Crashworthiness Due to Axial and Oblique Impact Forces. Thin-Walled Structures, 717–17.

TGHD, 2020. Traffic Accidents with Death and Injury by Types of Occuration in Turkey – 2020.

TurkStat, 2020. The Number of Road Motor Vehicles by Years, 2002-2020. Retrieved from https://data.tuik.gov.tr/Bulten/Index?p=Road-Motor-Vehicles-December-2020-37410

WHO, 2018. *Global Status Report on Road Safety*.

Xu, F., Yu, K., Hua, L., and Niu, X., 2021. Crashworthiness Design of Crash Box Filled with Negative Poisson's Ratio Based on Horn Structure. Mechanics of Advanced Materials and Structures, 0(0):1–18.

Yadav, V., 2006. *Finite Element Modeling and Side Impact Study of A Low-Floor Mass Transit Bus*. B. E. Shivaji University.

CURRICULUM VITAE

Umut Kumlu, graduated from Mehmet Akif Primary School in 2010 and graduated from Adana IMKB Anatolian Teacher High School in 2014. Then, he started his BSc degree in 2014 at Çukurova University, Automotive Engineering Department. He started his MSc education in Automotive Engineering Department of Çukurova University in 2019. He worked at Koluman Automotive Industry as R&D Engineer 2 years. He has been working as a Research Assistant in Çukurova University, Automotive Engineering Department since March 2021.